بِسْمِ ٱللَّهِ ٱلرَّحْمَٰنِ ٱلرَّحِيمِ

Sudan University of Science and Technology

College of Post Graduate Studies

The Effect of Dielectric Nano Size on its some Electrical and Optical Properties

تأثير الحجم النانوي لثنائي العزل الكهربائي على بعض خواصه الكهربية و الضوئية

Thesis Submitted for the Degree "Doctor of Philosophy"

Submitted by:

Amira Jad elrb Ali Fadl elmaula

Supervision by:

Professor Mubarak Dirar Abdullah

Co- Supervision Associated:

Doctor Ahmed Hassan Alfaki

March 2022

الآيـــــــة

بِسْـــمِ ٱللَّهِ ٱلرَّحْمَٰنِ ٱلرَّحِيـــمِ

﴿ وَقَالَ رَبِّ أَوْزِعْنِي أَنْ أَشْكُرَ نِعْمَتَكَ الَّتِي أَنْعَمْتَ عَلَيَّ وَعَلَىٰ وَالِدَيَّ وَأَنْ أَعْمَلَ صَالِحًا تَرْضَاه وَأَدْخِلْنِي بِرَحْمَتِكَ فِي عِبَادِكَ الصَّالِحِين﴾

سورة النمل(19)

Dedication

To those enlightened my way, urged me to succeed and encouraged me reach the highest goal.

To my parents

To my brothers and sisters

To my teachers and friends

Acknowledgment

Firstly my praise to Allah Whom blessed me with good health to complete this work.

I wish to express my sincere thanks and appreciation to my supervisor Prof. **Mubarak Dirar Abdullah** for his supervision and valuable guidance during the research period, his sincere technical advice and support that allowed me to complete this work.

I have to express my gratitude to the laboratories of Al-Neenlen University.

Thank also extend to department of physics, science college, graduate study college and Sudan university of science and technology.

List of Contents

List of table

List of Figures

Abstract

Nano optical and electrical properties play an important role in fabrication of new solar cells generation to solve the energy problem. To do this thin films fabricated from some magnetic materials were experimented. In this work, The ($Ba_xFe_{1-x}TiO_4$) (x=1, 0.1, 0.2, 0.3, 0.5, 0.6, 0.7,08, 0.9 and 0) were prepared by the sol- gel method. The influence of Fe concentration on the structural optical and electrical properties of the samples was studied by using x-ray diffraction (XRD), Reitveld and UV-VIS spectroscopy. It found the effect of iron doping improves the structural optical and electrical properties. The X-ray diffraction (XRD) analyses showed that for all samples the average Nano size decrease with decreasing of iron concentration. UV-visible absorption spectra showed that the observed value of the energy gap decreass from (2.074) eV to (2.046) eV as iron concentration decreases. The conductivity increases when Fe concentration increases for shorter wavelengths and decreases at long wavelength. Decreasing iron concentration increases absorption coefficient. Besides that decreasing Nano size, increases absorption coefficient. The results were explained according to electromagnetic and energy bands theories.

المستخلص

تلعب الخواص الضوئية و الكهربية للشرائح الدقيقة دوراّ مهماّ في تصنيع أجيال جديدة من الخلايا الشمسية لحل من مشكلة الطاقة للقيام بذلك تم إختبار شرائح دقيقة مصنعة من مواد مغنطيسية. في هذه الدراسة حضر المركب($Ba_xFe_{1-x}TiO_4$) لقيم (x= 1, 0.9, 0.8, 0.7, 0.6, 0.5, 0.4, 0.3, 0.2, 0.1 and 0) باستعمال طريقة السول– جل. ثم درس اثر تركيز الحديد على كل من الخواص التركيبية و الضوئية و الكهربية. الخواص التركيبية باستخدام جهاز حيود الاشعة السينية و وجد أن حجم جميع العينات في المدى النانوي. و أن معدل الحجم النانوي يقل بنقصان تركيز الحديد. كما حددت الخواص الضوئية و الكهربية باستخدام جهاز مطيافية الاشعة فوق البنفسجية و المرئية و وجد ان فجوة الطاقة تقل (من 2.074eV الى 2.046eV) . وأن الموصلية تزيد فى الاطوال الموجية القصيرة و تقل عند الاطوال الموجية الطويلة عند زيادة تركيز الحديد. كما أن نقصان تركيزه يؤدي لزيادة معامل الامتصاص. بجانب أن بنقصان الحجم النانوي يزيد معامل الامتصاص. حيث فسرت هذه النتائج على ضوء نظريات المجال المغنطيسي و نظرية النطاقات.

CHAPTER ONE

1.1 Nano Electronic

Nano science is a new branch of physics that emerges as a direct application of quantum physics. Nanotechnology is concerned with materials, structures, and systems whose components exhibit novel and significantly modified physical, chemical, and biological properties due to their nanoscale sizes [1].

The nanometer scale is conventionally defined as 1 to 100 nm. One nanometer is one billionth of a meter (10 m). The nanomaterial is considered to be a fundamental unit of nanotechnology. Nanomaterials are commonly defined as materials designed and produced to have structural features with at least one dimension of 100 nanometers or less. It can be formed in surface films (one dimension), strands or fibers (two dimensions), or particles (three dimensions) [2]. The change of geometry and nano size affects physical properties of nano materials. So there are wide ranges of material properties can be adjusted by structuring at the Nanoscale [3].

Actually nanomaterials have the structural features between of those of atoms and the bulk materials. As a consequence, the chemical (catalytic activity) and physical properties of nanomaterials (such as optical properties like absorption, refection, transition, optical absorption and fluorescence, electrical properties like conductivity electric permeability and resistivity, thermal properties, melting point and thermal conductivity, magnetism, etc.) are typically differ significantly from the corresponding bulk material[4].

A drastic change in the properties of nanomaterials is not just a step toward miniaturization, but requires consideration of many factors including their larger surface area to volume ratio, high surface energy, spatial confinement, reduced imperfections, lower melting point, lower phase transition temperature and reduced

lattice constants due to a huge fraction of surface atoms which provides possibilities for improvement of functionality of nanomaterials.

In addition to a change of properties of nano material basically on size affect, structure, composition and other several factor like a synthesis method, synthesis condition and synthesis parameters [5,6, 7,].

The nanomaterial can be prepared using wide variety of physical and chemical techniques. The bulk matter can be converted to nano matter by grinding or using solvent or even using laser [8].

Innovative nanoscale properties and functions will be achieved through the control of matter at the level of its building blocks: atom by atom, molecule by molecule, and nanostructure by nanostructure. Scientists develop new techniques to manufacturing nanoscale components and materials from larger starting materials or based on self-assembly of atoms and molecules. Accordingly synthesis method should exhibit control of size in this range so that properties can be controlled as well. Often the methods are divided into two main types, bottom up approach and top down [9, 10].

One of the major challenges in optimizing the optical and electrical properties of nanomaterials is the incorporation of doping ions into the nanomaterials lattice. Doping with selective elements offers an effective method to enhance and control the structural, electrical and optical properties of nanomaterials. [11].

Nano materials have unique, beneficial chemical, physical and mechanical properties and these properties are used for a wide range of applications for instance, in the field of electronics, optical communications technology, fuel cells, batteries, agriculture, food industry, and medicines.

This opens a new horizon in technology to produce new material types that can be property controlled to satisfy the required needs. One of the most promising applications is nano batteries and nano electronic components [11, 12, 13].

1.2 Research Problem

The intensive use of internet requires huge transmission of information. This makes the using of electronic circuits incapable to store and transmit the fastest for a large number of user's information. Nano science gives a powerful tool for controlling electric properties of matter. Using nano in integrated circuits the electronic devices can be made as small as possible.

1.3 Aim of the Work

The aim of this work is to see how changing the nano size of materials affects some of their optical and electrical properties.

1.4 Thesis Layout

The thesis consists of the five chapters. Chapter one is an introduction. Chapter two is the theoretical background about nano materials and their optical and electrical properties. Chapter three is the literature review. Chapter four consists of materials and experimental methods. Chapter five is concerned with results, discussion, conclusion and recommendations.

CHAPTER TWO

Theoretical Background

2.1 Introduction

This chapter consists of a theoretical part which describes, nanomaterials, the physical concepts to properties those have been studied in the research, and gives some mathematical relations and theories that used to calculate and discuss the results.

2.2 Nanomaterials

Nanoscale materials are defined as a set of substances where at least one dimension is less than approximately 100 nanometers. A nanometer is one millionth of a millimeter approximately 100,000 times smaller than the diameter of a human hair. Nanomaterials are of interest because at this scale unique optical, magnetic, electrical, and other properties emerge. These emergent properties have the potential for great impacts in electronics, medicine, and other fields [1, 13].

2.3 Classification of Nanomaterials

The nanomaterials are classified based on the dimension of nanomaterials, the origin of materials and based on materials used in the synthesis process.

2.3.1 On the Basis of Dimension

On the basis of dimension, nanomaterials are classified as:

i. **Zero Dimensional Nanostructures:** All dimensional at nanoscale nanoparticle (e.g. spheres, clusters etc.).

ii. **One Dimensional Nanostructure:** Two dimensional at nanoscale other dimensional not (e.g. nanowires, nanotube, nano rod etc.).

iii. **Two Dimensional Nanostructures:** One dimensional at nanoscale other two dimensional are not (e.g. nano film, nano coatings etc.).

iv. **Three Dimensional Nanostructures:** No dimensional at nanoscale nanoparticle, all dimensional at macro scale nanoparticle (e.g. particles, quantum dots, hollow spheres etc.) [2, 14].

2.3.2 Classification of Nanomaterials Based on Materials

1. **Carbon-Based Nanomaterials**

These types of nanomaterials are made up of carbon content and have various morphologies. The carbon-based nanomaterials can be hollow tubes or spheres, carbon nano fibers, Fullerenes, and graphene.

i. **Fullerenes:** Fullerenes are spherical carbon molecules made up of carbon atoms arranged in hybridization.

ii. **Graphene:** This is the carbon-containing network. The arrangement of carbon atoms forms a hexagonal pattern in the graphene network and makes two-dimensional planar surfaces.

iii. **Carbon Nano Tubes (CNTs):** These are nano foils made up of carbon-containing graphene.

iv. **Carbon Nano Fibers:** The graphene nano foils used in the production of carbon nano fibers are the same as CNTs but the structure is different [15, 16].

2. Inorganic-Based Nanomaterials

These nanomaterials are makeup metals and metal oxides; they can be synthesized from metals such as Ag, Au, and Fe; and the metal oxides are TiO_2, ZnO, and MnO_2.

Semiconductor nanomaterials are also synthesized from silicon and ceramic materials [2].

3. Organic-Based Nanomaterials

The organic-based nanomaterials are made up of organic matter other than carbon and inorganic material [15].

4. **Composite-Based Nanomaterials**

Composite nanomaterials are made up of one more layer of nanoparticles; these nanomaterials are combined with other nanoparticles, bulk materials, or more complex materials like metal frameworks. The composites may be made up of many types of materials such as metal, ceramic, organic, inorganic, carbon-based, bulk polymers or perovskites [17, 18].

2.4 Nanomaterial - Synthesis and Processing

Nanostructure materials have attracted a great deal of attention because their physical, chemical, electronic and magnetic properties show dramatic change from higher dimensional counterparts and depend on their shape and size. Many techniques have been developed to synthesize and fabricate nanostructure materials with controlled shape, size, dimensionality and structure. The performance of materials depends on their properties; these properties depend on the atomic structure, composition, microstructure, defects and interfaces which are controlled by thermodynamics and kinetics of the synthesis. There are two general

approaches to the synthesis of nanomaterials and the fabrication of nanostructures bottom-up approach and top-down approach [18, 19].

2.4.1 Bottom-Up Approach

The building of nanostructures starting with small components such as atoms or molecules is called bottom-up approach, example sol-gel, chemical vapour deposition (CVD), and physical vapour deposition (PVD) etc. [20].

1. **Sol- Gel Process**

In general, the sol-gel process involves the transition of a solution system from a liquid "sol" (mostly colloidal) into a solid "gel" phase. The starting materials used in the preparation of the "sol" are usually inorganic metal salts or metal organic compounds such as metal alkoxides. In a typical sol-gel process; the precursor is subjected to a series of hydrolysis and polymerization reactions to form a colloidal suspension, or a "sol". The starting material is processed to form a dispersible oxide and forms a sol in contact with water or dilute acid. Removal of the liquid from the sol yields the gel, and the sol- gel transition controls the particle size and shape. And heat treatment to transfer gel to solid. The gel formation depends on different parameters including the nature of starting materials (precursors), kind of solvent, alkoxy to water ratio, temperature of reaction, pH, stirring and aging time.

The sol –gel process can be summarized in three main steps.

1. Hydrolysis of precursors.

2. Gelation.

3. Drying [21].

2. Chemical Vapour Deposition (CVD) Method

Chemical vapour deposition (CVD) method involves a transport of reactant gases towards the substrate kept at some temperature where reactants crack in to different products; which diffuse on the surface and undergo certain chemical reactions at appropriate site nucleate and grow to form desired films, coatings, wires and tubes.

The system follows a four step mechanism for any type of CVD.

1. Transport of precursors into the reactors.

2. Absorption and diffusion of precursors on the substrate.

3. Chemical reactions at the substrate.

4. Deposition and growth of film [22, 23].

3. Physical Vapour Deposition (PVD)

Physical vapour deposition (PVD) is a technique by which a metal, ceramic or a compound can be converted into gaseous form and then deposited on the surface of a substrate.

In general, PVD methods are subdivided into:

1. Evaporation

The source materials used in this process are generally refractory metals such as W, Ta, Mo etc. In evaporation technique, both substrate and source materials (to be deposited) are placed inside the vacuum chamber. The vacuum is required to allow the molecules to evaporate and to move freely in the chamber. An electron gun (e-gun) is used to produce electron beam of 10 Kev; this beam is directed at

the source material in order to develop sufficient vapour so as to produce deposits on wafer or substrates [24].

2. Sputtering

The source materials used in this process are generally an alloy, ceramic or a compound. In sputtering technique, a high energy atom in ionized form usually Ar+ is used to hit the surface atoms of the targeted source material. Then the knocked out atoms in vapour form are deposited on the surface of the substrate to produce a uniform coatings [19, 25].

3. Pulsed Laser Deposition or Laser Ablation Pulsed

Pulsed laser deposition (PLD) is a thin film deposition technique that is used to deposit materials on substrates. A base system consists of a target, substrate carrier which is mounted in a vacuum chamber. An excimer laser is used to energize the surface of a target to produce a deposition plume. The plume is typically directed towards the substrate where a thin-film is deposited. Since each shot of the laser is directly related to the amount of material ablated, the deposition rate can be calibrated and controlled very precisely [26].

2.4.2 Top-Down Approach

The process of making nanostructures starting with larger structures and breaking away to nano size is called top-down approach. The most widely used by top–down methods for nanomaterial synthesis mechanical milling, and etching [20].

1. **Mechanical Milling**

The mechanical ball milling technique is generally beneficial for the synthesis of various types of nano material such as metallic and ceramic nano materials. In

this the balls rotate with high energy inside a container and then fall on the solid with gravity force and kinetic and hence crush the solid into nano crystallites [27].

2. Etching

Etching is used to reveal the microstructure of metal through selective chemical attack; it also remove thin, highly deformed layer introduced during grind and polishing. In general, there are two classes of etching processes: wet etching where the material is dissolved when immersed in chemical solution and dry etching where the material is sputtered or dissolved used reactive ion or a vapor phase etchant.

2.5 Crystal Structure Properties

Crystals are solid chemical substances with a three dimensional periodic array of atoms, ions, or molecules; this array is called a crystal structure. A crystal structure is composed of a unit cell; a set of atoms arranged in a particular way; which is periodically repeated in three dimensions on a lattice. The spacing between unit cells in various directions is called its lattice parameters. The symmetry properties of the crystal are embodied in its space group. A crystal's structure and symmetry play basically role to determine many of crystal properties, such as, electronic band structure, and optical properties. The crystal structure studies through the diffraction of photon, neutron and electron [28, 29].

Most methods for determining the atomic structure of crystals are based on the idea of scattering of radiation. X-rays is one of the types of the radiation which can be used. The wavelength of the radiation should have a wavelength comparable to a typical interatomic distance which is in solids of a few angstroms (10^{-8} cm). There are a number of various setups for studying crystal structure using x-ray diffraction. In most cases, the wavelength of radiation is fixed, and the angle

is varied to observe diffraction peaks corresponding to reflections from different crystallographic planes. Using the Bragg law one can be determine the distance between the planes.

In 1913 Bragg found that crystalline solids have remarkably characteristic patterns of reflected x-ray radiation. In crystalline materials, for certain wavelengths and incident directions, intense peaks of scattered radiation were observed. Bragg accounted for this by regarding a crystal as made out of parallel planes of atoms, spaced by distance d apart. The conditions for a sharp peak in the intensity of the scattered radiation were that: the incident waves are reflected specularly from parallel planes of atoms in the crystal with each plane reflecting only a very small refraction of the radiation, like a lightly silvered mirror. In specular (mirror like) reflection the angle of incidence is equal to the angle of reflection. The diffracted beams are found when the reflection from parallel planes of atoms interferes constructively.

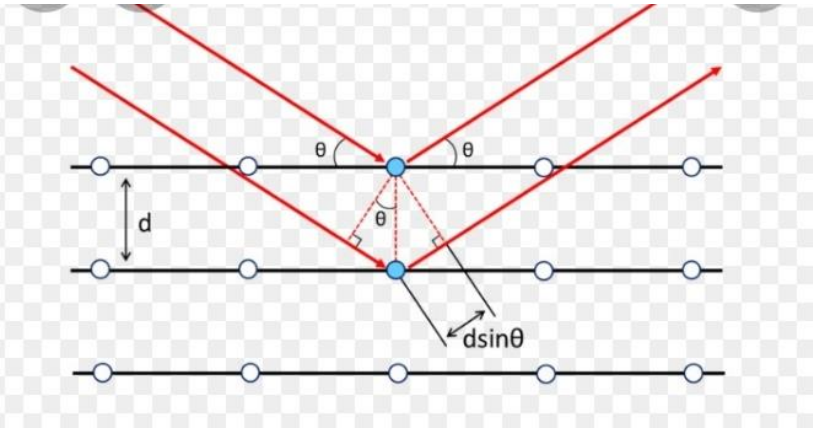

Figure (2.1): Shows X-rays which are specularly reflected from adjacent planes.

The path difference between the two x-rays is equal to 2dsinθ. For the x-rays to interfere constructively this difference must be an integer number of wavelengths. This leads to Bragg the condition:

$$2d \sin\theta = n\lambda \quad (2.1)$$

The integer, n is known as the order of the corresponding reflection (or order of interference).

The crystal structure can characterized by its, six lattice constant(axial lengths a, b, c or angle α, β, γ), geometrical shape and size , Density, space group, atomic positions**(** primitive or no primitive**)**, distance between atoms(d-space) and points of plane intercepts on three axes(Miller indices)[28,29]. We shall define them in the follows paragraphs.

2.5.1 Unit Cell

Unit cell is smallest possible portion or part of crystal lattice which repeats in different directions of lattice; it can be characterized by its lattice parameters, the length of the cell edges and the angles between them, while the positions of the atoms inside the unit cell are described by the set of atomic positions (x_i, y_i, z_i) measured from a lattice point. The types of unit cell;

i. **Primitive Unit Cell:** Which the constituent particles are present only at the corners of the unit cell.
ii. **Centered Unit Cell:** Which the constituent particles are present at other with corners of the unit cell.
iii. **Body – Centered:** When the constituent particles is present at the body center along with corners of the unit cell.
iv. **Face - Centered:** If the constituent particles are present at the six face center along with corners of the unit cell.
v. **Ended - Centered:** If the constituent particles are present at the centers of any two opposite faces along with corners of the unit cell [30].

2.5.2 Lattice Parameters

The spacing between unit cells in various directions is called its lattice parameters or lattice constants. Parameters either a measure of axial lengths (a, b, c) or angle (α, β, γ) that defines the size and shape of unit cell of crystal lattice [31].

2.5.3 Crystal Shape

Shape of crystal is an external appearance of the crystal is often related to its internal arrangement of atom; it may be monoclinic, triclinic, cubic, tetragonal, hexagonal and orthorhombic. These Shapes are determined by a number of factors such as length of their faces and edge as well as the angle between them. The edge lengths of a crystal are represented by letters a, b, and c. the angles at each faces intersect are represented by the Greek letters α, β, and γ. Each of the crystal systems differs in terms of the angles between the faces and the number of edges of equal length on each faces.

2.5.4 Miller Indices

The orientation of a plane in a lattice is specified by Miller indices; which are defined as follows: Group of three numbers that indicates the orientation of a plane or set of parallel planes of atoms in a crystal; they acts as the smallest integral multiples of the reciprocals of plane intercepts on three axes.

So to determine Miller indices of plane along each of the three crystallographic directions the following:

For any crystal a lattice vector can be written as that given by:

$$T = n_1 a_1 + n_2 a_2 + n_3 a_3 \quad (2.2)$$

Where $[n_1\ n_2\ n_3]$ are integers number.

First find intercept of the plane with the axes along the primitive translation vectors a_1, a_2 and a_3. Let's these intercepts be x, y, and z, so that x is fractional multiple of a_1, y is a fractional multiple of a_2 and z is a fractional multiple of a_3. Therefore we can measure x, y, and z in units a_1, a_2 and a_3 respectively. We have then a triplet of integers (xyz). Then we invert it (1/x 1/y 1/z) and reduce this set to a similar one having the smallest integers by multiplying by a common factor. This set is called Miller indices of the plane (h k l).For example, if we have a plane which intercepts the axes at (2, 3, 2), its reciprocal is (1/2, 1/3, 1/2), and scaling (multiply by 6 in this case) results in (3, 2, 3). These are the Miller indices. If the intercept is negative, put a bar over the index. For example, for intercepts (−3, 2, 2), we will have indices ($\bar{2}$, 3, 3). If the plane is parallel to an axis, its intercept will be at infinity; hence its index will be 0. Planes with Miller indices (h, k, l) are parallel to those with (n h, n k, n l), for any integer n [30, 32].

2.5.5 D-Space

The d-space can be described as the distance between planes of atoms that give rise to diffraction peaks. Each peak in diffractogram results from a corresponding d – space.

It can be calculated from formula as Bragg's law [28, 30]:

$$n\lambda = 2d\sin\theta$$

$$d = \frac{n\lambda}{2\sin\theta} \qquad (2.3)$$

Where: n is order of reflection.

λ: Wave length (0.01 – 10 nm).

θ: Peak position.

d: distance between planes of atoms.

2.5.6 Density of Unit Cell

Density of unit cell is given as the ratio of mass and volume of unit cell.

Density of unit cell=$\frac{\text{Mass of unit cell}}{\text{Volume of unit cell}}$

Mass number of unit cell= number atoms of unit cell × mass of one atom =n × m (g).

But mass of one atom (m) =$\frac{\text{atomic mass}}{\text{avogadro numbers}} = \frac{M}{N_A}$

Density of unit cell;

$$\rho = \frac{n \times M}{V \times N_A} \text{ gcm}^{-3} \quad (2.4)$$

n is number of atoms associated with each unit cell.

M is atomic weight.

V is volume of the unit cell.

N_A is Avogadro's number (16.022×10^{23} (atoms/mole) [33].

2.5.7 Crystallite Size

Crystallite size is the smallest most likely single crystal in the powder form. Most commonly the crystallite size is determined by measuring the Bragg peak width at half the maximum intensity and putting its value in Scherer's formula which is mentioned below [34]:

Scherer's formula:

$$x_s = \frac{0.9\lambda}{B \cos\theta} \quad (2.5)$$

Where:

x_s is the crystallite size, λ is the wavelength of the X-radiation used, B is the peak width at half the maximum intensity, and θ is the Bragg angle.

2.5.8 Symmetry in Crystal

Symmetry operations include:

1. Rotation axes; which rotate the structure a specified number of degrees, and a center of symmetry in-fold rotation (Cn), rotation by 360º/n (n = 1, 2, 3, 4, 6)

2. Mirror planes; which reflect the structure across a central plane, Mirror plane.

3. Inversion point; which inverts the structure through a central point [35].

2.5.9 The Space Group

The space group of the crystal structure is composed of the Bravais lattice type and translational symmetry operations.

To write natation for space group:

First sample is represents the Bravais lattice type; P: primitive, A, B, C: base centered, I: body centered, R: rhombohedral and F: face centered, and then followed symmetry element N_n/: the first symbol is N_n; N: 2, 4 or 6 (2-flod, 4-flod or 6-flod) and second symbols is be joined by slash is symmetry operations (mirror planes m and a glide plane n).When the first symbol is 2, 4 or 6 and second symbols is be joined by slash, as in 2/m, 4/m, and 6/m; this meaning of 2-flod, 4-flod or 6-flod axis with mirror plane perpendicular to it. For example the space group $P4_2$ /mnm as we found in our prepared samples P indicated a primitive Bravias lattice screw axis, m indicates mirror planes and n indicates a glide plane [36, 37, 38].

2.6 Physical Properties of Nanomaterials

Nano materials have the structural features in between of those of atoms and the bulk materials. The properties of materials with nanometer dimensions are significantly different from those of atoms and bulks materials. Two fundamental factors, both related to the size of the individual nanocrystal are responsible for these unique properties. The first is the large surface to volume ratio, due to their small dimensions; which makes a large to be the surface or interfacial atoms, resulting in more "surface" dependent material properties. Especially when the sizes of nanomaterials are comparable to length, the entire material will be affected by the surface properties of nanomaterials. This in turn may enhance or modify the properties of the bulk materials. And the second factor is spatial confinement effect on the materials, which bring the quantum effects.

The various properties, which altered due to the size reduction in at nanometer, are: thermal, mechanical, magnetic, electronic and optical properties. Many applications of the nanomaterials rose from these unique properties [39, 40]. We will discuss optical and some of electronic properties with detail.

2.6. 1 Thermal Properties

Thermal properties explain the response of materials to application of heat. Thermal properties like melting point, thermal conductivity and heat capacity. Reduction of particle size from micron to nanometer scale influences the thermal properties like melting point and thermal conductivity. The melting point of a material directly correlates with the bond strength. In bulk materials, the surface to volume ratio is small and hence the surface effects can be neglected. However, in nanomaterials the melting temperature is size dependent and it decreases with the decrease particle size diameters. The reason is that in nanoscale materials, surface

atoms are not bonded in direction normal to the surface plane and hence the surface atoms will have more freedom to move. This is drastically altering on their thermodynamic and thermal properties [19, 41].

2.6.2 Mechanical Properties

Mechanical properties are physical properties exhibits upon the application forces. Examples are the modulus of elasticity, tensile strengths, hardness, and flexibility. The nanoscale size of the nanomaterials tends to modify many of the mechanical properties of nanostructured materials from the bulk materials. An enhancement of mechanical properties of nanomaterials generally results from structural perfection of the materials [42].

2.6.3 Optical Properties

Optical property of a material is defined as its interaction with electromagnetic radiation in the visible. Optical properties of materials are essential for optical science research and industrial applications. The interaction of light with matter is different at different wavelengths and the techniques to measure the optical properties differ based on the spectral region of interest.

The optical properties exhibited by nanomaterials are quite different from their bulk counterpart. The reason behind this change in property is mainly due to the effect of the surface. In addition to, the increased energy level spacing is also an important criterion for this changing behavior, which effect by doping and interaction with the surrounding environment or other nanostructures [43, 44].

2.6.3.1 Processes of Light:

When radiation interacts with matter, a number of processes can occur; including reflection, scattering, absorbance, Fluorescence, and photochemical reaction (absorbance and bond breaking).

The crystals are composed of charged particles: bound and conduction electrons, ionic cores, impurities, etc. These particles move differently with oscillating electric fields, giving rise to polarization effects. At visible and infrared light frequencies, the only contribution to polarization comes from the displacement of the electron cloud, which produces an induced dipole moment. According to that the charged particles obey on the equations of motion, and they give rise to fields in accordance with Maxwell's theory of electrodynamics. The interaction of the electromagnetic radiation with these crystals is treated, by applying the boundary conditions to the solutions of the Maxwell equations at the boundary between the different media.

Maxwell equations [45]:

$$\mathrm{H} - \frac{1}{\mathrm{C}}\frac{\partial \mathrm{D}}{\partial \mathrm{t}} = \frac{4\pi}{\mathrm{C}}\mathrm{J}$$

$$\nabla \times \mathrm{E} + \frac{1}{\mathrm{C}}\frac{\partial \mathrm{B}}{\partial \mathrm{t}} = 0$$

$$\nabla \cdot E = 0$$

$$\nabla \cdot B = 0 \qquad (2.6)$$

1. Reflection of Light

When light passes from one transparent medium to another having a different index of refraction, some of it is reflected off a surface (such as a mirror), since the

angle of incidence on a reflecting basic surface is equal to the angle of reflection (reflection law).

2. Refraction of Light

When light is incident at interface, the geometrical plane that separates one optical medium from anther, it will be partly reflected and partly transmitted and refracted into second medium. The bending waves of light at interface between two optical mediums called refraction.

3. Transmission of Light

The transition of light, that intensity of light transmitted out of the substance. The quantity related with transmission of light is transmittance; which means quantity of light that is passes through sample. Transmittance is determined by the relationship between amount of light that is transmitted (I) and original (I_0) of light this expressed in following formula:

$$T = \frac{I}{I_0} \tag{2.7}$$

4. Absorption of Light

Absorption is light which absorbed by sample. The quantity related with absorption of light is absorbance which means amount of light absorbed by sample.

Absorbance is determine by the relationship between amount of light that original (I_0) of light is and transmitted light (I) this expressed in following formula [46, 47,48]:

$$A = \frac{I_0}{I} \tag{2.8}$$

Beer – Lambert law is discussed relationship between the amount of light transmitted and the thickness of the sample. It was stated that, the absorbance of a

solution is directly proportional to the thickness and the concentration of the sample, as follows:

$$A = \alpha ct \tag{2.9}$$

Where: A is absorbance.

C is concentration.

t is path length (thickness).

α is absorbance coefficient or molar absorptivity ($Lmol^{-1}\ cm^{1}$)

In spectrophotometry the absorbance and transmittance are often related together. The ray of light with intensity (I_0) comes into material, the material will absorb part of the light (I_a) and the other remaining light will transmit (I_t). That expresses as follows:

$$I = I_a + I_t \tag{2.10}$$

When using percentage transmittance values, it is easy to relate and to understand the numbers. For example, 50% transmittance means that half of the light is transmitted and half is absorbed, while 75% transmittance means that three quarters of the light is transmitted and one quarter absorbed. Completely transparent substance will have $I_t=I_0$ and its Transmittance is will be 100% and its absorbance is zero. Similarly a substance which no allow radiation of particular wavelength to pass through it will $I_t=0$ and corresponding to zero percent transmittance and its absorbance is 100%. Thus the relationship between absorbance (α) and Transmittance (T) can be expressed by the following [49, 50]:

$$A = \frac{1}{T} = \frac{I_0}{I} \tag{2.11}$$

Absorbance (A), then, is defined as the logarithm (base 10) of the reciprocal of the transmittance.

$$A = -\log_{10} T$$

$$A = -\log_{10}\left(\frac{I}{I_0}\right) \tag{2.12}$$

The Beer – Lambert law in exponential formula can be written as following:

From (2.9) and (2.12),

$$A = -\log_{10}\left(\frac{I}{I_0}\right) = \alpha c t$$

For concentration one mole, c=1.

$$A = \log_{10}\left(\frac{I}{I_0}\right) = -\alpha t \tag{2.13}$$

Light loses intensity in absorbed material according Beers law given as following:

By take the exponential for equation (2.13):

$$\frac{I}{I_0} = e^{-\alpha t}$$

This equation may be rewrite as,

$$I = I_0 e^{-\alpha t} \tag{2.14}$$

Where α is absorbance coefficient.

t is thickness of matter.

I_0, I, are intensity of absorption and transition light.

The absorption coefficient α can be related to the band gap. Tauc derived an expression that gives the relation between absorption coefficient α and the incident photon energyhυ. According the fallowing relation:

$$\alpha h\upsilon \propto \Delta E^n \tag{2.15}$$

Absorption operation depends on energy of photon hυ and energy gap E_g. If energy of photon hυ equal to energy gap E_g, photon will absorbed to generate pairs of electron –hole. If energy of photon hυ less than energy gap E_g, photon will not absorbed. If energy of photon hυ greater than energy gap E_g, electron will exiting from valance band to conductor band since the difference in energy $h\upsilon - Eg$ will released in heat form [28, 51,52];

$$\Delta E = h\upsilon - E_g \tag{2.16}$$

From (2.15) and (2.16),

$$\alpha h\upsilon = c\left(h\upsilon - E_g\right)^n \tag{2.17}$$

Where hυ is the photon energy.

Eg is the optical band gap (the threshold for photons to be absorbed).

c is a proportionality constant depend on sort of matter.

n is the index indicating the type of transition.

2.6.3.2The Optical Constants

Optical constants any several quantities characteristic of the optical behavior of substance as refractive index, absorption coefficient, dielectric constant, extinction coefficient and optical conductivity, which are response coefficients of matter to an incident electromagnetic wave of circular frequency ω. The optical constant will vary for different wave lengths, so it can be used to predict the material's response to each wave length [53].

1. The Absorption Coefficient (α)

The absorption coefficient (α) measures the intensity loss of the electromagnetic radiation, as it passes through substance [54, 55].

The absorption coefficient can be obtained by taken the logarithm for equation (2.14):

$$\log_{10}\frac{I}{I_0} = -\alpha t \log_{10} e$$

By substitute equation (2.12):

$$A = \alpha t \log_{10} e$$

$$\alpha = \frac{A}{t\log_{10} e} = \frac{2.303A}{t}$$

$$\alpha = \frac{2.303A}{t} \qquad (2.18)$$

2. Extinction Coefficient

Extinction coefficient is measure of light lost due to scattering and absorption per unit distance of the penetration medium. It can be obtained from the following equations [56]:

Starting with electric field formula;

$$E(z,t) = E_0 e^{i(Kz-\omega t)} \qquad (2.19)$$

The value of wave number given by:

$$k = \frac{2\pi}{\lambda/_n} = \frac{n\omega}{c} \Rightarrow k = n\frac{\omega}{c}$$

And the value of wave velocity given by:

$$\frac{2\pi}{\lambda/_n} = \frac{n\omega}{c} \Rightarrow \omega = \frac{2\pi c}{\lambda} \qquad (2.20)$$

n is complex index, which include two important optical properties index, n_0 is the real part; related to the refraction, and k_0 is the imaginary part; related to the attenuation of incident light (extinction coefficient).

So complex index of refraction of the medium n is defined as:

$$n = n_0 + ik_0 \tag{2.21}$$

$n_0$is real index refraction.

$k_0$is extinction coefficient.

Then k from equation (2.21) became:

$$k = (n_0 + ik_0)\frac{\omega}{c} \tag{2.22}$$

Substitute equation (2.22) in equation (2.19)

$$E(z,t) = E_0 e^{i\left(\frac{(n_0+ik_0)\omega z}{c}-\omega t\right)}$$

$$= E_0 e^{\frac{-k_0\omega z}{c}} e^{i\left(\frac{\omega n_0 z}{c}-\omega t\right)}$$

$$= E_0 e^{\left(\frac{-k_0\omega z}{c} + i\left(\frac{\omega n_0 z}{c}-\omega t\right)\right)} \tag{2.23}$$

The complex conjugate of electric field given by:

$$E^* = E_0 e^{\left(\frac{-k_0\omega z}{c} - i\left(\frac{\omega n_0 z}{c}-\omega t\right)\right)} \tag{2.24}$$

The intensity of absorption proportional with electric field and conjugate of electric field:

$$I \propto EE^*$$

Then intensity of absorption from equation (2.23) and (2.24) gives as:

$$I \propto E_0 e^{\left(\frac{-k_0 \omega z}{c} + i\left(\frac{\omega n_0 z}{c} - \omega t\right)\right)} \cdot e^{\left(\frac{-k_0 \omega z}{c} - i\left(\frac{\omega n_0 z}{c} - \omega t\right)\right)}$$

$$I \propto E_0 e^{\left(\frac{-2k_0 \omega z}{c}\right)} \quad (2.25)$$

By comparative equation (2.25) with equation (2.14), here z is acts the thickness t, the absorption coefficient(α)equals:

$$\alpha = \frac{2k_0 \omega}{c}$$

Then substitute the value of ω from equations (2.20),

$$\alpha = \frac{2k_0 \omega}{c} = \frac{4\pi k_0}{\lambda} \quad (2.26)$$

So the extinction coefficient (k_0) equals:

$$k_0 = \frac{\lambda \alpha}{4\pi} \quad (2.27)$$

3. Refraction Index

The refractive index (n) is the relative between speeds of light in vacuum to its speed in material which does not absorb this light. The value of n can be calculated from the equation [57.58].

$$n = \left[\left(\frac{(1+R)}{(1-R)}\right)^2 - (1 + k_0^2)\right]^{\frac{1}{2}} + \frac{(1+R)}{(1-R)}\Bigg] \quad (2.28)$$

Where (R) is the reflectivity.

k_0 is extinction coefficient

4. Dielectric Constant

As electromagnetic wave interacts with dielectric medium, polarization of the medium occurs and this is dependent on the permittivity of the medium. To find

out what kind of electromagnetic waves exist inside the dielectric medium, use Maxwell equations obtains the well-known formula for refractive index under assumptions that there are no free charge $\nabla \cdot E=0$, no currents $\nabla \cdot B=0$and all materials are non-magnetic $\mu=0$incase Maxwell equations reduce to wave vector equations the solution will be propagating wave [59,60];

$$\nabla^2 E-\frac{\varepsilon}{c^2}\frac{\partial^2 E}{\partial t^2}=0$$

$$\nabla^2 B-\frac{\varepsilon}{c^2}\frac{\partial B}{\partial t}=0 \qquad (2.29)$$

The solutions to these equations, we assume that electric field has the form of harmonic plane waves with the wave vector k,

$$E = E_0 \exp i(\omega t - kz) \qquad (2.30)$$

Where ε is relative permittivity, c is the velocity of light, E_0 is amplitude, and ω is wave velocity.

Substitute equation (2.29) in equation (2.30) and diffraction in z direction;

$$(-ik)^2 e^{i(\omega t-kz)} - \frac{\varepsilon}{c^2}(i\omega)^2 e^{i(\omega t-kz)} = 0$$

$$k^2 + \frac{\varepsilon}{c^2}\omega^2 = 0 \implies \omega = ck\varepsilon^{-\frac{1}{2}} \qquad (2.31)$$

The phase velocity of the wave

$$v = \frac{\omega}{k} = \frac{c}{n} \qquad (2.32)$$

From (2.31) and (2.32):

$$v = \frac{\omega}{k} = c\varepsilon^{\frac{-1}{2}} = \frac{c}{n}$$

$$c\varepsilon^{\frac{-1}{2}} = \frac{c}{n} \tag{3.33}$$

The equation (2.33) can be written as follows:

$$\varepsilon = n^2 \tag{2.34}$$

This indicates the dielectric constant is directly related to the optical properties.

In general, the dielectric constant ε refraction is complex quantities, that is,

$$\varepsilon = \varepsilon_1 + i\varepsilon_2 \tag{2.35}$$

$\varepsilon_1$is real dielectric constant.

$\varepsilon_2$is imagery dielectric constant.

From equation (2.21), equation (2.34) and equation (2.35),

$$\varepsilon_1 + i\varepsilon_2 = (n_0 + ik_0)^2 = n_0^2 + 2nki - k_0^2$$

$$\varepsilon_1 + i\varepsilon_2 = n_0^2 + 2n_0\, k_0 i - k_0^2 \tag{2.36}$$

Thus from equation (2.36)

The real Dielectric Constant (ε_1)

$$\varepsilon_1 = n_0^2 - k_0^2 \tag{2.37}$$

The imaginary dielectric constant (ε_2)

$$\varepsilon_2 = 2n_0\, k_0 \tag{2.38}$$

5. Optical Conductivity

The optical conductivity is a measure of frequency response of material when irradiated with light.

The dielectric constant is related to the optical conductivity. To derive the relation between the dielectric constant and the optical conductivity, we assume that electric field is oscillating with angular frequency ω.

$$E(z,t) = E_0 e^{i(Kz-\omega t)} \tag{2.39}$$

This wave propagates through the medium with conductivity σ (ω) and the dielectric constant ε (ω), both being the function of ω. This implies the polarization of the medium occurs only due to the bound charges (polarization due to ions). The electric current and the electrical displacement are related to the electric field by the fallows relations [61, 62],

$$J = \sigma E$$

$$D = \varepsilon E \tag{2.40}$$

We could start with the equation of motion for electrons:

$$\nabla^2 E = \frac{\varepsilon\mu}{C^2}\frac{\partial^2 E}{\partial t^2} + \frac{4\pi\sigma\mu}{C^2}\frac{\partial E}{\partial t} \tag{2.41}$$

$$\nabla^2 H = \frac{\varepsilon\mu}{C^2}\frac{\partial^2 H}{\partial t^2} + \frac{4\pi\sigma\mu}{C^2}\frac{\partial H}{\partial t} \tag{2.42}$$

Substitute equations (2.39) and (2.40) in equation (2.41) and take the diffraction in z – direction.

$$-k^2 = -\frac{\varepsilon\mu\omega^2}{C^2} - \frac{4\pi i\sigma\mu\omega}{C^2} \tag{2.43}$$

We may rewrite equation (2.43) in the form

$$k^2 = \frac{\omega^2}{C^2}\mu(\varepsilon + \frac{4\pi i\sigma}{\omega}) \tag{2.44}$$

If there were no losses (or no attenuation), k would be equal to

$$k_0 = \frac{\omega}{c}\sqrt{\varepsilon\mu} \tag{2.45}$$

And would be real, but since there are losses we write

$$k = \frac{\omega}{c}\sqrt{\varepsilon_{complex}\mu} \tag{2.46}$$

Where we have defined the complex dielectric function as

$$\varepsilon_{complex} = \varepsilon_1 + i\varepsilon_2 = \varepsilon + \frac{4\pi i\sigma_{opt}}{\omega} \tag{2. 47}$$

So the imaginary dielectric part

$$\varepsilon_2 = \frac{4\pi\sigma_{opt}}{\omega}$$

Then optical conductivity from equation(2.47)

$$\sigma_{opt} = \frac{\varepsilon_2\omega}{4\pi} \tag{2.48}$$

By substitute $\varepsilon_2$from equation (2.38)

$$\sigma_{opt} = \frac{2n_0\, k_0\omega}{4\pi}$$

$$\sigma_{opt} = \frac{2k_0\omega n_0}{4\pi} \tag{2.49}$$

The absorption coefficient from equation (2.26) equals,

$$\alpha = \frac{2k_0\omega}{c}$$

$$\alpha c = 2k_0\omega \tag{2.50}$$

Then optical conductivity can be obtained by:

$$\sigma_{opt} = \frac{\alpha c n_0}{4\pi} \tag{2.51}$$

2.6.4 Electrical Properties

Electrical properties of materials are their ability to conduct electrical current. Various electrical properties such are resistivity, electrical conductivity and dielectric sterngth.

Reduction in material's dimensions would have effects on electrical properties. In bulk materials, conduction of electrons is delocalized, that is, electrons can move freely in all directions. When the scale is reduced to nanoscale, the quantum effect dominates. For zero dimensional nanomaterials, all the dimensions are at the nanoscale and hence the electrons are confined in three dimensional spaces. Therefore no electron delocalization (freedom to move) occurs. For one dimensional nanomaterial, electrons confinement occurs in two dimensional spaces and hence electron delocalization takes place along the axis of nanotubes, Nano rods, or nanowires. In the case of two dimensional nanomaterials, the conduction electrons will be confined across the thickness but delocalized in the plane of the sheet. Due to electron confinement, the energy bands are replaced by discrete energy states which make the conducting materials to behave like either semiconductors or insulators [63]. Here we shall discuss two important electrical properties related to spectroscopy studies;

1. Electric Conductivity

The electrical conductivity is measure of materials ability to allow the transport of an electric charge. It can be estimated using the following relation [64].

$$\sigma_{ele} = \frac{2\lambda\sigma_{opt}}{\alpha} \tag{2.52}$$

2. Permittivity

Permittivity is measure of well the molecules of substance align polarize under electric field. This value calculated from the relation:

$$\varepsilon_r = \frac{8.85x10^{-12}}{\sqrt{n}} \tag{2.53}$$

where n is refractive index.

2.6.5 Magnetic Properties

Magnetic property refers response of material to an applied magnetic field. The magnetic property of solid known as magnetism arises from dipole moment in solids. This dipole moment appears from the spinning of electrons in its axis and orbital motion around the nucleus of atom. The magnetic properties of solid are observed due to the magnetic field created by electrons, magnetic moment and electric current.

1. Permeability

Magnetic permeability is property exhibit by the material where the material allows of magnetic lines of force to pass through it. It can be calculated from the relation [33, 65]:

$$\mu_r = \frac{\sqrt{n}}{1.257x10^{-6}} \tag{2.54}$$

where n is refractive index.

2.7 Band Theory of Solid

The optical and electrical properties of solid materials determine by energy bands structure and occupied with electrons.

The energy band structure of a solid determines whether it is a conductor, an insulator or a semiconductor. A solid contains an enormous number of atoms packed closely together. Each atom, when isolated, has a discrete set of electron energy levels 1s, 2s, 2p.... If we imagine all the N atoms of the solid to be isolated from one another, they would have completely coinciding schemes of their energy levels.

Let us study what happens to the energy levels of an isolated atom, as they are brought closer and closer together to form a solid. If the atoms are brought in close proximity, the valence electrons of adjacent atoms interact. Hence the valence electrons constitute a single system of electrons common to the entire crystal with overlapping of their outermost electronic orbits. Therefore, the N electrons will now have to occupy different energy levels. This is brought about by the electric forces exerted in each electron by all the N nuclei. As a result of these forces, each atomic energy level is split up into a large number of closely spaced energy levels. A set of such closely spaced energy levels is called an energy band.

In the energy band, the allowed energies are almost continuous. These energy bands are in general, separated by regions, which have no allowed energy levels. These regions are known as "forbidden bands" or 'energy gaps'. The amount of splitting is not the same for different levels. The levels filled by the valence electrons in an atom are disturbed to a greater extant, while those filled by inner electrons are disturbed only slightly.

If there are N atoms in a solid, there will be N allowed quantum states in each band. Each quantum state can be occupied by a maximum of two electrons with opposite spins. Thus each energy band can be occupied by 2N electrons.

The band formed from the atomic energy levels containing valance electrons is called valance band. These electrons have the highest energy. Above the valance band, there is the band of next higher permitted energies called (the conduction band). The conduction band corresponds to the first excited states; electrons can move freely in this band and are called (conduction electrons). The interval between conduction band and valence band in which electrons cannot occupy is called (Forbidden gap).

Impurities and point defect generate additional energy level in the forbidden band gap of ideal crystal. If impurities atoms are quite far from each other, interaction between them is absent, and correspondence to those energy level is discrete. If impurities atoms are quite close to each other, their valence orbits can overlap, and discrete energy levels split to the impurity energy bands. And this factor can enable conductance, if not all the levels in the band are occupied [28, 66].

2.8 Zeeman Effect

It is well known that an atom can be characterized by a unique set of discrete energy states.

If there is a magnetic field influence on atom, the atomic energy levels are split to a large number of levels. This effect is known as the Zeeman Effect.

The origin of Zeeman Effect is the following. In an atomic energy state, an electron orbits around the nucleus of the atom and has a magnetic dipole moment associated with its angular momentum. In a magnetic field, it acquires an additional energy just as a bar magnet does and consequently the original energy level is shifted and will split into several energy levels with different energies.

In this effect the intensity of magnetic field causes change in electron energy in level k (E_k) and became:

$$E = E_k + E_1 = E_k + V_m \tag{2.55}$$

Where V_m is additional energy.

To determine these energy levels with different energies use perturbation theory independent time. Whereas additional energy(E_k) equals to magnetic potential energy (V_m);

$$V_m = \int Fds = \int Frd\,\theta$$

When the magnetic field is present. Consider a magnetic dipole that happens to be at an angle θ to the direction of the magnetic field. The magnetic field produces a torque μ × B on the magnetic dipole. Since the torque is perpendicular both to μ and B, the change in the angular momentum will also be perpendicular, causing the magnetic dipole to process around the magnetic field.

$$V_m = \int qBrd\theta = \int (qr)Bd\theta$$

$$= \int \mu B d\theta$$

$$\int \tau d\theta = \int (\mu B) d\theta = \int (\mu B \sin\theta) d\theta$$

$$\tau = \mu B \sin\theta$$

$$V_m = -\mu B \cos\theta \tag{2.56}$$

If we imagine the atoms as systems of electrons orbiting round protons, they can certainly give rise to magnetism. Which maintains that an electric current (I), going round in a plane will produce a magnetic moment [61, 67]:

$$\mu = IA \tag{2.57}$$

Where A is the area of the current loop. If the current is caused by a single electron rotating with an angular frequencyf, then the magnetic moment becomes:

$$\mu = (-ef)(\pi r^2) \tag{2.58}$$

Where r is the radius of the circle.

Introducing now the angular momentum,

$$L = mvr = m(\omega r)\, r$$

$$= m(2\pi fr)\, r = m(2\pi f)r^2$$

$$= -\frac{2m}{e}(-ef)(\pi r^2) \tag{2.59}$$

From equation (2.58) and (2.59),

$$L = -\frac{2m}{e}\mu \tag{2.60}$$

We may rewrite in equation (2.60) in the form:

$$\mu = -\left(\frac{e}{2m}\right)L \tag{2.61}$$

Substitute this in equation (2.56)

$$V_m = \left(\frac{e}{2m}\right)\, L\, B\cos\theta \tag{2.62}$$

For magnetic in the z – direction,

$$\cos\theta = \frac{L_z}{L} = \frac{\hbar\, m_l}{\hbar\sqrt{l(l+1)}}$$

$$= \frac{m_l}{\sqrt{l(l+1)}} = \frac{m_l}{L}$$

$$L\cos\theta = m_l \tag{2.63}$$

Then magnetic potential energy,

$$V_m = \left(\frac{e}{2m}\right) B m_l \tag{2.64}$$

Magnetic quantum number, $m_l = 0, \pm 1, \pm 2,..$

Accordance to perturbation theory we found that:

$$E_1 = (H_1)_{kk} = \int \overline{u_k} V_m u_k dr$$

$$= V_m \int \overline{u_k} u_k dr = V_m$$

$$E_1 = V_m \tag{2.65}$$

Thus From equation (2.64) additional energy equals:

$$E_1 = \left(\frac{e\hbar}{2m}\right) B m_l$$

$$E = E_k + E_1$$

$$E = E_k + \left(\frac{e\hbar}{2m}\right) B m_l \tag{2.66}$$

Where, $m_l = 0, \pm 1, \pm 2,..$

Thus the level E splits to a number of levels according to value ofm_l.

m_l= 1,

$$E = E_k + \left(\frac{e\hbar}{2m}\right)B$$

$m_l = -1$,

$$E = E_k - \left(\frac{e\hbar}{2m}\right)B$$

2.9. Properties of Absorption Spectrum for Infrared Radiation

Infrared radiation is widely used in industry, scientific research, medicine and military technology. Recording of emission and absorption spectra in the IR range (their spectroscopy) is used in study of structure of the electron shell of atoms, for the purpose to determine the molecular structure, as well as chemical bond between atoms [68].

Infrared radiation that portion of the electromagnetic spectrum that extends from long wavelength or red, end the visible light range to the microwave range. Invisible to human eye, it can be detected as sensation of warmth on skin. It divided into three regions; the near-, mid-and far-infrared, named for their relation to the visible spectrum.

1. The far-infrared, approximately 400-10cm-1(1000–30μm), lying adjacent to the microwave region, has low energy and may be used for rotational spectroscopy.
2. The mid-infrared, approximately 4000-400cm-1(30–1.4μm) may be used to study the fundamental vibrations and associated rotational-vibrational structure.
3. The higher energy near-IR, approximately 14000-4000cm-1(1.4–0.8μm) can excite overtone or harmonic vibrations. The names and classifications of

these sub regions are merely conventions. They are neither strict division nor based on exact molecular or electromagnetic properties.

An infrared spectroscopy is study the interaction of infrared light with matter. The fundamental measurement obtained in infrared spectroscopy is infrared spectrum, which is plot infrared intensity versus wavelength or frequency of light.

Infrared spectrum can be characterized by its energy E (J), wavelength λ (μm), frequency v (Hz) or wavenumber (cm-1); the number of waves per unit of distance. There are related to each other through:

$$E = h\upsilon . c = \frac{hc}{\lambda} \qquad (2.67)$$

Where h is Plank's constant (6.63·10-34 J·s), and c is the velocity of the radiation in vacuum (2.9979·108 m/s).

The wavelength and wave number are related to each other via the following equation:

$$\upsilon = \frac{1}{\lambda} \qquad (2.68)$$

The equation above shows that light wave may be described by their wavelength, and wave number or frequency. Here we typically refer to light waves by their wave number, however it will be more convenient to a light wave's wavelength or frequency [69].

2.9.1 The Absorption Band of Infrared

When radiation passes through a sample, part of the radiation may be absorbed by the sample provided that there is a change in the dipole moment during the vibration. The dipole moment of such a molecule changes as the bond expands and contracts.

There are two conditions for molecule to absorb infrared light:

The first necessary condition for molecule to absorb infrared light is that the molecule must vibration during which the change in the dipole moment with respect to distance is non-zero. This condition can be summarized in equation:

$$\frac{\partial \mu}{\partial x} \neq 0 \tag{2.69}$$

The second necessary condition for infrared absorbed is that energy of light impinging on molecule equal vibrational energy level difference within molecule. This condition can be summarized in equation:

$$\Delta E = hc\upsilon \tag{2.70}$$

ΔEis vibrational energy level difference in molecule.

h is Plank's constant (6.63·10-34 J·s), and c is the velocity of the radiation in vacuum (2.9979·108 m/s). υis wave number.

If energy of photon does not meet the criterion in this equation, it will be transmitted by the sample and if energy of photon satisfies this equation, the photon will be absorbed by the molecule.

The interactions of infrared radiation with matter may be understood in terms of changes in molecular dipoles associated with vibrations and rotations. In order to begin with a basic model, a molecule can be looked upon as a system of masses joined by bonds with spring-like properties. Then atoms in the molecules can also move relative to one other, that is, bond lengths can vary or one atom can move out of its present plane. This is a description of stretching and bending movements that are collectively referred to as vibrations.

For a diatomic molecule, only one vibration that corresponds to the stretching and compression of the bond is possible. Hooke's law:

$$\upsilon = \frac{1}{2\pi c}\left(\frac{k}{\mu}\right)^{\frac{1}{2}} \tag{2.71}$$

Hence υ wave number, k is force constant and μ is reduced mass, which may be expressed as follows:

$$\mu = \frac{m_1 m_2}{m_1 + m_2} \tag{2.72}$$

The equation (2.71) give the frequency of light that molecule will absorb, and give the frequency of vibration of normal mode exited by light [70]

2.9.2 Intensity of Absorption Band of Infrared

There are many factors effects on intensity of absorption band of infrared**:**

Two variables as mention in equation (2.72); which used to explain the effect of frequency of vibrational modes are atomic masses and force constant. The others are bond strength, electronegativity and concentration of sample.

i. Chemical bond's force constant: No two substances have same force constant and reduce mass. The two molecular properties determine at which a molecule will absorb infrared light. Force constant is directly proportional with wave number, greater force constant greater wave number, and then it has higher intensity of absorption band.
ii. Reduces mass is inversely proportional with wave number, thus lighter masses have large wave number than heavier masses, then it has higher intensity of absorption band.
iii. Bond strength: this depends on long of bond atoms. Atoms with shorter distance bond; have higher amount of the dipole moment then it has

higher intensity of absorption band. Atoms with tri bond is longer than that double bond and single,

$$\mu = qx \tag{2.73}$$

Where μ is dipole moment, q is electron charge and x is distance between atoms long of bond.

iv. Electronegativity: This is measure of the tendency of atom to attract electrons towards it. Higher electronegativity higher intensity of absorption band.

v. Another factor that determines the peak intensity of in infrared spectra is the concentration of molecule in the sample. The equation that relates concentration to absorbance is beers law.

2.9.3 Types of Molecular Vibration

1. Stretching Vibration

The stretching vibration in which the distance between two atoms around a bond is varies with time. They are of two types, symmetrical and unsymmetrical.

i. In the symmetrical stretching vibration, the side atoms move away from the central atom along the molecular axis and, after reaching maximum displacement, move back toward the central atom.

ii. In the asymmetrical stretching vibration, one side atom approaches the central atom while moving back from the other.

2. Bending Vibrations

In the bending (deformation) vibration, the angle between two atoms varies with time [71].

2.10 Perovskite

Perovskite is considered one of the most promising materials of the twenty-first century. In the past few decades, the perovskite has attracted broad attention and made great progress in energy storage, as well as optoelectronic devices due to its superior photoelectric and catalytic properties [72].

A natural perovskite a type of mineral that was first found in Ural Mountains. It was discovered by Gustav Rose in 1839 and named after Russian mineralogist Count Lev Alekseevich Perovski (1792–1856).

Perovskite is calcium titanium oxide or calcium titanate, with the chemical formula CaTiO3. All materials with the same crystal structureasCaTiO3, namely ABX3 structure are collectively referred to as perovskite materials, where A and B are cations. A is usually an alkaline or rare earth element, and B transition metals. While X is anion may be oxide or halogen. This can be simply divided into inorganic perovskite and organic-inorganic hybrid perovskite.

Materials with perovskite-type are of considerable interest in matter sciences as well as advanced materials research and applications. This is due to their wide array of properties. The ample variety of functional properties of the perovskite materials arises from the range of different crystal structures they may adopt by incorporating different alkaline earth, rare-earth, and transition metal ions.

Perovskite materials are widely used for scientific and technological applications. It can be applicable to design developed electronic devices due to its remarkable electronic properties. The perovskite materials are well known for several significant properties like ferroelectric, piezoelectric, magneto caloric and optical, dielectric and ferromagnetic properties etc. [73].

Basically, properties of the perovskite material are depended on the structure, composition and other several factor like a synthesis method, synthesis condition and synthesis parameters. A wide range of perovskite material properties can be adjusted by structuring at the Nanoscale.

Generally, Nano-sized perovskite are prepared by solid-state reactions, a hydrothermal reaction etc. Sol-gel auto combustion has recently become a very popular technique due to simple process, low sintering temperature, and time and energy consumption than other traditional methods. Therefore, the sol-gel method is employed to improve properties with more homogeneity and constricted particle distribution this will be making an impact on structural, electrical and optical properties of perovskite [74].

The family of perovskite materials has all kind of compounds including metals, semiconductors, insulators, and superconductors which make them applicable in various technologies.

2.10.1 Types of Perovskites

Perovskites have different types**.**

1. Simple perovskites like KMnF3 and SrTiO3.
2. complex perovskites: which is arise as result of adopt by incorporating different alkaline earth, rare-earth, and transition metal ions in the A and B sites of their basic ABO3 unit cell.

2.10.2 Properties of Perovskite Materials

Depending on which atom or molecules are used in the structure, the resulting perovskites can have many different properties including:

1. **Superconductivity:** Is characterized by zero electrical resistance and expulsion of magnetic fields occurring in certain materials when cooled below a characteristic critical temperature
2. **Optoelectric Property:** Which convert optical to electrical and electrical to optical.
3. **Giant Magnetoresistance:** It has ability to change resistance under influence of magnetic field.
4. **Ferroelectric:** Is defined as the spontaneous alignment of electric dipoles by their mutual interaction in the absence of an applied electric field. Thus ferroelectric materials must possess permanent dipoles. Example barium titanate ($BaTiO_3$), Rochelle saltand potassium niobate (KNo_3).
5. **Piezoelectric: Piezoelectric:** is defined as polarization induced by the application of external force. Hence piezoelectric materials, have ability to convert mechanical stress into electrical energy. For example; barium titanate ($BaTiO_3$), lead titanate and quartz [75, 76].

2.10.3. Perovskites for Devices

Perovskite has been widely used in many fields due to the great progress in material and device preparation technology such as Solar cells Photo detectors devices.

1. **Solar Cells**

Perovskites are considered to be the most promising candidates for solar cells due to their excellent diffusion length (more than 1 μm), low preparation temperature, low cost, and high efficiency.

2. **Photo detectors**

Photo detectors, which could convert incident light into electrical signal, are very important optoelectronic devices for optical communications, homeland security, and environmental monitoring. Many works have reported that perovskite-based photo detectors have the abilities to sense the spectra from deep-UV to visible and NIR and even to X-ray or γ ray [75, 77].

Chapter Three

Literature Review

3.1 Introduction

Electronic devices with suitable size, high quality and application encourage scientists to search for many techniques to synthesize and fabricate materials with controlled shape, size, dimensionality structure and unique properties of matter. One of most promising ones is fabricate materials in Nano size. In this chapter will display some of these all tempts.

3.1.1 Effect of Iron Doping on the Structural and Optical Properties of CeO_2 Films

This work was done by Duangdao Channei1, Auppatham Nakaruk, Sukon Phanichphant, Pramod Koshy and Charles Christopher Sorrell. In this work undoped and Fe-doped CeO_2thin films were fabricated by spin coating on F-doped tin oxide glass substrates followed by annealing at 500°C for 15 h. The concentration of the dopant was varied from 2 to 10 % iron by weight (metal basic).

The thickness of the films was determined by dual-beam focused ion beam milling to be 150 nm for undoped film, while Fe-doped CeO_2films have thickness of 200 nm for all dopant samples. The transmission spectra from UV–visible spectrophotometry showed a red shift of the absorption edge of the doped films, and the optical indirect band gap of the films decreased from 3.48 to3.20 eV with increasing dopant concentration. The mineralogical data showed that doping $CeO_2$with Fe3 resulted in a significant lowering of the transmission of the films in

the visible range, although this could be attributed to increased absorption and reflection from the films due to the associated change in color of the films. The decrease in crystallinity of the films with increased dopant concentration is attributed to precipitation of the dopants on the grain boundary which would hinder the recrystallization of CeO_2. This decreased crystallinity could also explain the lowering of transmission due to increased scattering from the amorphous structure [78]. We observed that his study agrees with our study by effect of dopant increasing absorption and decrease the energy gap. But we found that occurs as decreasing Fe concentration. This may be explained by assuming that the magnetic field generated by Fe acts against the net crystal forces that increase and broaden energy bands, which decreases the energy gap. The decreases of energy gap increases absorption and absorption coefficient this may be attributed to the fact that decreasing the energy gap allows longer wave length beside the shorter wave lengths to be absorbed by electron to move from the valence to the conduction band.

3.1.2 Synthesis of Iron-Doped TiO_2 Nanoparticles by Ball-Milling Process: the Influence of Process Parameters on the Structural, Optical, Magnetic, and Photocatalytic Properties

This work was done by J. O. Carneiro•S. Azevedo, F. Fernandes, E. Freitas, M. Pereira, C. J. Tavares, and S. Lanceros-Me´ndezand, V. Teixeira Titanium dioxide (TiO_2) absorbs only a small fraction of incoming sunlight in the visible region thus limiting its photocatalytic efficiency and concomitant photocatalytic ability. The large-scale application of TiO_2 nanoparticles has been limited due to the need of using an ultra violet excitation source to achieve high photocatalytic activity. The inclusion of foreign chemical elements in theTiO_2 lattice can tune its band gap resulting in an absorption edge red-shifted to lower energies enhancing

the photo-catalytic performance in the visible region of the electro-magnetic spectrum. In this research work, TiO_2 nanoparticles were doped with iron powder in a planetary ball-milling system using stainless steel balls. The correlation between milling rotation speeds with structural and morphologic characteristics, optical and magnetic properties, and photocatalytic abilities of bare and Fe-doped TiO_2 powders was studied and discussed. The study observed that, the angular position of some XRD peaks was slightly shifted after Fe-doping, thus indicating some distortions of TiO_2 crystal lattice promoted by the iron dopant. For the non-milled TiO_2. However, after being subjected to different ball-milling rotation speeds, the sample experienced some variations in its IEP. The band-gap energy for the un-milled/pure TiO_2 nanoparticles is higher in comparison with the obtained values for the milled/pure TiO_2 ones, decreasing with the increase of the rotation speed. Moreover, the band-gap energy for the Fe-TiO_2nanoparticles is still lower than the milled/pure TiO_2samples [79]. In this study agrees with our study at the result of effect the increasing of Fe dopant, decreases the band-gap energy.

3.1.3 Effect of Iron Doping on Structural and Optical Properties of TiO_2 Thin Film by Sol–Gel Routed Spin Coating Technique

This work was done by Stephen Lourduraj and Rayar Victor Williams. Thin films of iron (Fe)-doped titanium dioxide (Fe: TiO) powered prepared by sol–gel spin coating technique and further calcined at 450C. The structural and optical properties of Fe-doped TiO_2 thin films were investigated by X-ray diffraction (XRD), scanning electron microscopy (SEM), ultraviolet–visible spectroscopy (UV–vis) and atomic force microscopic (AFM) techniques. The XRD results confirm the nanostructured TiO_2 thin films having crystalline nature with anatase phase. The characterization results show that the calcined thin films having high crystallinity and the effect of iron substitution lead to decreased crystallinity. The

SEM investigations of Fe-doped TiO_2 films also gave evidence that the films were continuous spherical shaped particles with a nano metric range of grain size and film was porous in nature. AFM analysis establishes that the uniformity of the TiO_2 thin film with average roughness values. The optical measurements show that the films having high transparency in the visible region and the optical band gap energy of Fe-doped TiO_2 film with iron (Fe) decrease with increase in iron content. These important requirements for the Fe: TiO_2 films are to be used as window layers in solar cells [80]. This study shows that the effect of iron substitution on the high crystallinity of thin lead to decreased crystallinity, and the optical band gap energy of decrease with increase in iron content. While we observed that the decreasing of crystal sizes and the optical band gap energy as result of decreasing of Fe concentration. This may be explained by assuming that decreasing Fe concentration which has atoms acts as magnetic dipoles decreases repulsive magnetic force, which decreases crystal spacing and crystal size.

3.1.4 Effect of Particle Size on Band Gap and DC Electrical Conductivity of TiO_2 Nanomaterial

This work was presented by BS Avinash, VS Chaturmukh, HS Jayanna, and CS Naveen. Material to the nano scale can exhibit different properties compared that they exhibit on micro scale, enabling unique applications. When TiO_2 is reduced to nano scale it shows that unique properties, which is the electrical aspect is highly important. This paper presents increase in energy gap and decrease in conductivity with decrease in particle size of pure nano TiO_2. Synthesized by hydrolysis and piptization of titanium isopropoxide. Aqueous solution with various pH and peptizing the resultant suspension will form nano TiO_2 at different particle sizes. As the pH of the solution is made acidic reduction in the particle size is observed. And it is confirmed from XRD using Scherer

formula and SEM, as prepared samples are studied for UV absorbance, and DC conductivity from room temperature to 400 C. from the Tauc plot it was observed, and calculated the energy band gap increases as the particle size decreases and shown TiO_2 is direct band gap. From Arrhenius plot clearly we encountered, decrease in the conductivity for the decrease in particle size due to hopping of charge carriers and it is evident that, it can tailor the band gap by varying particle size [81]. In our research it found that increases conductivity although the energy gap increases. In this case may be result from the fact that increasing Fe concentration decreases the energy gap, thus allows more electrons to bridge the energy gap.

3.1.5 Structural and Optical Properties of Fe-Doped Ruddlesden – Popper $Ca_3 Ti_{2-x}Fe_x O_{7-\delta}$ Nanoparticles

This work was presented by L.H Omari and H. Lassri. In this work, the ruddlesden – popper perovskite $Ca_3 Ti_{2-x}Fe_x O_{7-\delta}$ (x=0.0, 0.02, 0.04, 0.06 and 0.08 (CTF_xO)) powders were synthesized by sol gel route. The crystal structure was examined using X-ray diffraction (XRD) and shows that the Fe doping induces a negligible structural change without perturbing their original crystal structure. The optical properties were investigated by uv–visible spectroscopy. The results indicate that x=0.08 of Fe doping at the B-site in $Ca_3Ti_{2-x}Fe_xO_{7-\delta}$ (CTO) reduces the optical band gap from 3.61 to 2.23 ev. Hence Fe substitution induces disorder and broadens the gap edge of absorption significantly that can makes these materials as promising candidate in photovoltaic application. Furthermore different fundamental optical properties such as the transmittance, optical band tial, refractive index, optical conductivity, and dielectric coefficient were determined and correlated to the variation of Fe content. Moreover, they have examined the influence of Fe doping on nonlinear optical (NLOp) properties of the studied

compounds and they exhibit an enhanced nonlinear optical behavior with increasing Fe content [82]. The result indicates that Fe doping reduces the optical band gap agrees with my work**.**

3.1.6 Effect of Concentration of Reactants on the Optical Properties of Iron Doped Cadmium Stannate Thin Films Deposited by Spray Pyrolysis

This work was done by Nicholas O. Ongwen, Andrew O.Oduor1, and Elijah O. Ayieta. In this work spray Pyrolysis Technique was used in depositing thin films of cadmium stannate, doped with iron metal. The precursor solutions used were sprayed onto the preheated glass slides that were kept at a constant temperature of 450°C. The transmittance and reflectance measurements were made in the spectral wave length range of 300 -1100nm. It was found out that both the concentration of the reactants and doping had an effect on the optical properties of the deposited thin films. At the upper end of the visible spectrum (718nmwavelength), the values of the optical constants were: Transmittance of up to 70.45%, thickness of 323–594nm, refractive index of 2.108–3.542, absorption coefficient of 7.385 x103cm -1–2.2784cm-1, and extinction coefficient of 0.042cm–0.130cm and band gap energy of 3.9 eV. They observed that the transmittance of the deposited TF's increased with increase in the wave length. The absorption coefficient was observed to increase with increase in the photon energy, increasing sharply at high energies above3.8eV. The film thickness increased with increase in the concentration of Cd_2 SnO_4. When heavily doped, the thickness of the TF's was also observed to increase with increase in the concentration of Cd_2 SnO_4. However, the thickness of the heavily doped TF's was lower than that of the undoped TF's. The absorption coefficient generally increased with increase in the concentration of the precursor solutions (film thickness), both for the undoped and the heavily doped TF's. The extinction coefficient was found to increase sharply at

low wave lengths below 320nm (high energies above 3.8eV). The extinction coefficient was also observed to increase with increase in the concentration of Cd_2 SnO_4. On doping, the extinction coefficient was observed to increase also. The refractive index generally decreased with increase in the wave length. At longer wavelengths, the refractive index tended to be constant. The refractive index was also observed to increase with increase in concentration of Cd_2 SnO_4. The real part of the dielectric constant was found to reduce with increase in wavelength. At longer wavelength, the dielectric constant tended to be constant. The dielectric constant also increased with increase in the concentration of Cd_2 SnO_4. Upon doping, the dielectric constant also increased. A band gap energy of3.9eV was obtained for both the undoped and the heavily doped TF's [83]. In our study we also observed that the absorption coefficient was increase with increase in the photon energy, but the effect of Fe dopant, was different, whereas absorption coefficient increases as Fe decreases.

3.1.7 Structural, Optical Spectroscopy, Optical Conductivity and Dielectric Properties of $BaTi_{0.5}$ $Fe_{0.33}$ $W_{0.17}$ O_3Perovskite Ceramic

This paper was presented by Faycal Bourguibal, Ahmed Dhahri, Tarek Tahri, Kamel Taibi, Jemai Dhahrii, and Ekhlil. In this paper material ($BaTi_{0.5}$ $Fe_{0.33}$ $W_{0.17}$ O_3) was prepared by a solid-state reaction method. Structural and optical properties of this ceramic compound have been studied by X-ray diffraction, scanning electron microscopy and spectroscopy ellipsometry. Rietveld analysis of XRD data shows the mixture phases (cubic double and hexagonal) of crystal structure at room temperature, and the particle sizes observed by SEM are larger than those calculated by XRD, The optical properties of BTFW have been investigated by SE. The refractive index of the BTFW increases and then it decreases when the photon energy increases. The extinction coefficient also increases when photon energy

increases. The absorption coefficients increase quickly with increase in photon energy. The optical absorption coefficient α of BFTW, which is calculated from the ellipsometric data, has shown a high value around the fundamental absorption edge and reflects the good quality of our sample. The direct optical band gap energy was estimated to be~4.36 eV. The optical conductivity (σ opt), the complex electric modulus (M) and the complex impedance (Z) of this ceramic were calculated optically. This opens the door to control the structural and the optical properties of perovskite materials and leads to important industrial applications such as: solar cells, electronic and optoelectronic devices with a low price [84]. We also found that the absorption coefficients increase with increase in photon energy.

3.1.8 Study Structural and Optical Properties of Cd Se: Al Thin Films as a Function of Doping Ratio and Annealing Temperature

This work was presented by Abbas Hiader Hussein. In this work, study the structural and optical properties of pure Cadmium Selenide (Cd Se) thin films, which prepared by thermal evaporation under vacuum method and also study the influence of doping by Aluminum (Al) with different ratios on the structural and optical properties of Cadmium Selenide (Cd Se) thin films. The results showed that the value of optical energy gap decreases with increasing doping percentage. The optical constants which represented by (refractive index, extinction coefficient and dielectric constant in its two parts) are also calculated in this research. And found increase in extinction coefficient and refractive index value with the increase in the doping percentage [85]. However we study the effect of ($Ba_x Fe_{1-x} Ti O_4$) Nano size on physical properties. The results showed that the value of optical energy gap decreases as decreases Fe doping. This may be also explained by assuming that the magnetic field generated by Fe acts against the nano crystal forces that increase and breaded energy bands, which breaded decreases the energy gap.

3.1.9 Characterization Techniques of Fe-Doped CuO Thin Films Deposited by the Spray Pyrolysis Method

This work was studied by Fatima Zahra Chafi, Lahoucine Bahmad, Najem Hassanaini, Boubker Faresi, and Larbi Laanab. In this study Fe-doped CuO thin films were deposited onto glass substrates by Spray pyrolysis technique. The structural, micro-structural, optical and electrical properties of the synthesized samples were investigated in details. The X-Ray diffraction (XRD), Raman and Fourier Transform Infrared (FTIR) spectroscopy, confirmed that the studied samples exhibit single phase monoclinic structure of CuO. The UV-VIS spectrophotometer mentioned that the transmittance increases to 80 % when increasing the Fe concentration. Furthermore, the band gap energy of the obtained CuO was 1.29eV.This value was slightly increased by the Fe substitution. In addition, the electrical properties of the films such as the conductivity, the mobility, the resistivity and the carrier concentration have been studied. The Hall Effect measurements confirmed the p-type conductivity of the studied films. The increase of the optical band gap when increasing the Fe doping amount might be explained by the decrease of the grain sizes. Hence, the electrical part unveiled a significant increase in the conductivity and the mobility within an increase in Fe-doping content. A decrease in the resistivity and the carrier concentration of the films is investigated. It confirmed that the growth in the films is p-type in nature [86]. We observed that the result of the optical band gap which reported by this study agrees with our result, hence for both study there is direct relation between optical band gap and Fe doping concentration.

3.1.10Multiferroic Fe^{3+} ion doped $BaTiO_3$ Perovskite Nano Ceramics: Structural, Optical, Electrical and Dielectric Investigations

This work was presented by Dhananjay N. Bhoyar, Sandeep B. Somvanshi, P. B. Nalle1, V. K. Mande, A.A. Pandit, and K. M. Jadhav. In the present investigation, nano crystalline $Sr_{0.5}$ $Ba_{0.5}$ $Ti_{1-x}Fe_x$ O_3 (x = 0.00, 0.15, 0.20) nanoparticles (BST) were synthesized by sol-gel auto combustion method. The effect of iron (Fe) doping on the structural, electric and dielectric and optical properties examined by the X-Ray diffraction (XRD), two probe and UV-vis techniques. XRD analysis shows that prepared samples are in a single phase with the tetragonal structure at room temperature. Structural parameters like average crystallite size (D) and lattice constant (a and c) were calculated from the XRD data. The surface morphology of the samples was studied by field emission scanning electron microscopy (FE-SEM) technique. It was found that the nanoparticles are cubic in shape for parent BST nanoparticle whereas Fe doped shows tetragonal shape. Energy dispersive spectrum (EDS) reveals that compositional elements are in stoichiometry proportion. The DC electrical resistivity measurements of the prepared samples were carried out in the temperature range of 300–850 K using a standard two-probe method. The electrical resistivity (ρ) decreases with temperature and Fe concentration. The frequency was measured at room temperature in the frequency range of 30Hz to 1MHz. The dielectric parameters show strong compositional as well as frequency dependence. The higher values of dielectric parameters were found at lower frequencies. UV-visible absorption spectra showed that absorption edge shifted to higher wavelength with increasing Fe concentration while corresponding energy band gap of the prepared nano ceramics decreases with increasing Fe concentration [87].

3.1.11 Influence of Fe-Doping on the Structural and Optical Properties of ZnO Thin Films Prepared by Sol–Gel

This work was done by Linhua Xua and Xiangyin Li. In this work, Fe-doped Zn O thin films were prepared by sol–gel method on Si and glass substrates and influence of Fe-doping concentration on the structural and optical properties of the films was studied. The X-ray diffraction (XRD) analyses show that all the ZnO thin films prepared in this work have a hexagonal wurtzite structure and are preferentially oriented along the c-axis perpendicular to the substrate surface. After 1 at% Fe is doped, the crystalline quality and the preferential orientation of ZnO thin film are improved. However, when Fe-doping concentration is above 1 at%, the crystalline quality and the preferential orientation of ZnO thin film is weakened in turn. The surface morphology analyses of the samples show that the ZnO grain sizes tend to decrease with the increase of Fe-doping concentration. Fe-incorporation hardly influences the transmittance in the visible range, but the optical band-gaps of ZnO thin films gradually increase with the improved Fe-doping concentration. The photo luminescence spectra display that all the samples have an ultraviolet emission peak centered at381 nm and the 1 at% Fe-doped ZnO thin film has the strongest ultraviolet emission peak. The above results suggest that 1 at% Fe-incorporation can improve the crystalline quality and enhance the ultraviolet emission of ZnO thin film [88].

Chapter Four

Materials and Experimental Method

4.1. Introduction

This chapter is concerned with the experimental work, which includes Materials, sample preparation and techniques uses. In this work ten samples of (Ba_x $Fe1_{-x}TiO_4$) were prepared.

4.2 Materials

1. Barium Nitrate [Ba $(NO_3)_2$]

Barium nitrate is chemical compound. Its molecular formula Ba $(NO_3)_2$,Molar mass 261.35**,** physical state solid (crystalline)**,** Color White crystals, density 3.24 g/cm³ at 20 °C**,** melting point: freezing point at 592 C**,** and moderately soluble in water.

2. Iron (III) Nitrate [Fe $(NO_3)_3.9HO_2$]

Its molecular formula $Fe(NO_3)_3$ * 9 H_2O, Molar mass 404 g/mole, physical state solid (crystalline), color light: brown, melting point: freezing point47 °C, density 1.68 g/cm³ at 20 °C ,and solubility: soluble in water.

3. Titanium Dioxide (TiO_2)

Its molecular formula (TiO_2**)**, molar mass 79.866 g/mole, physical state solid, color white, melting point: freezing point 1,843°C, Density 4.23 g/cm³, and solubility: insoluble.

4. Nitric Acid

Its molecular formula HNO_3, molar mass 63.012 g/mole, physical state (liquid), color: colorless, melting point -42°C, density 1.5129g/cm³ °C, and solubility: completely miscible.

5. Distilled Water

Distilled water is steam from boiling water that's been cooled and returned to its liquid state. It's the purest water.

4.3 Synthesis of ($Ba_xFe_{1-x}TiO_4$) Nano Powder

The ($Ba_xFe_{1-x}TiO_4$) (x=1, 0.1, 0.2, 0.3, 0.5, 0.6, 0.7,08, 0.9 and 0) powders were prepared by the sol- gel method. Barium nitrate [$Ba(NO_3)_{2]}$], Iron(III) nitrate [$Fe(NO_3)_3.9HO_2$] and titanium oxide were used as starting material, distilled water as dissolving medium and nitric acid as adjusting of PH less than 5 PH .

First Barium nitrate and Iron nitrate were weighted by taking suitable quantity of them, then each one solved separately in distilling water to make solution. After that the solution was stirred and heated after PH was adjusted to 5.0 at$70c^0$ for one hour.

The volume of distilling water was determined by the molarity equation:

$$M_0 = \frac{n}{V_w \times 1000}$$

Since,

$$n = \frac{W_g}{W_m}$$

$$V_w = \frac{W_g}{M_0 \times 1000 \times W_m}$$

Where: n is number molar.

$W_g$is weight by gram of sample.

$V_w$is volume of water.

W_m is the molecular weight.

$M_0$is the molecular concentration.

Secondly the two solutions were mixed and added 3.0g of titanium oxide, the product mixture was heated and stirred at $70c^0$ continuously about one hour, the last one was deposited for one day then filtered to obtain pure solution (Hydrolysis step), which was slowly evaporated to form sol by continues in heat treatment convert to gel at$150c^0$ after two hours (gelation step). Finally the gel was dried and grinded to powder.

Figure (4.1): The solution form of ($Ba_xFe_{1-x}TiO_4$) (x = 1, 0.1, 0.2, 0.3, 0.5, 0.6, 0.7,08, 0.9 and 0) samples.

Figure (4.2): Sol form for one sample of ($Ba_xFe_{1-x}TiO_4$) (x = 1, 0.1, 0.2, 0.3, 0.5, 0.6, 0.7,08, 0.9 and 0) samples.

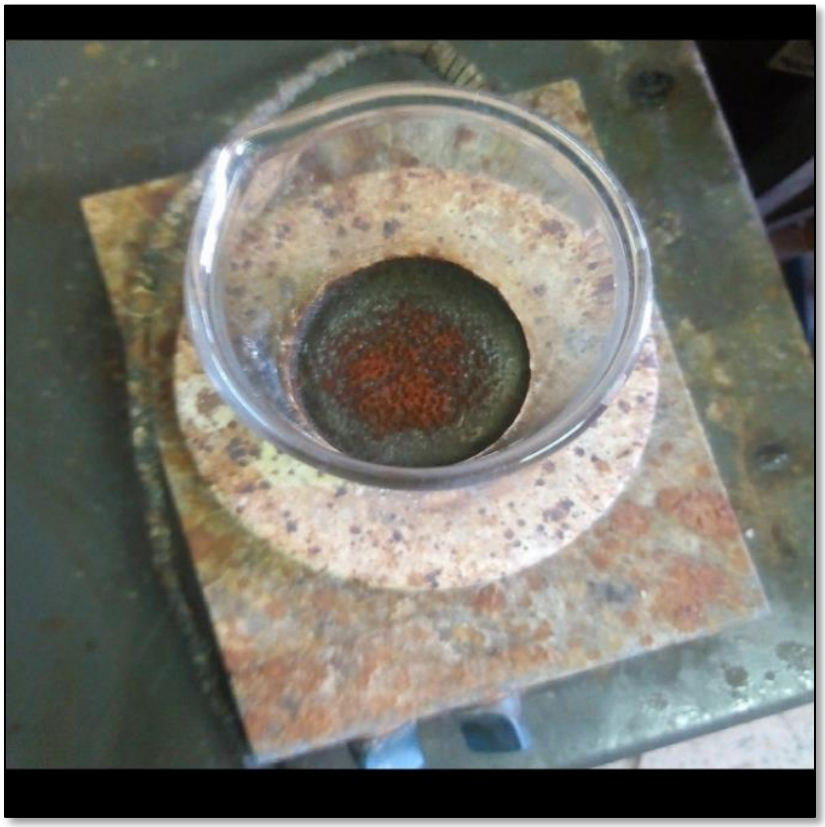

Figure (4.3): Gel form for one samples of ($Ba_xFe_{1-x}TiO_4$) (x= 1, 0.1, 0.2, 0.3, 0.5, 0.6, 0.7,08, 0.9 and 0) samples.

Figure (4.4): Nano powder form for two samples of ($Ba_xFe_{1-x}TiO_4$) (x= 1, 0.1, 0.2, 0.3, 0.5, 0.6, 0.7,08, 0.9 and 0) samples.

4.4 Techniques Uses

The structure of the samples was characterized by X-ray diffraction (XRD) and the optical properties were investigated by using UV-visible absorption spectrophotometer

4.4.1 X-ray Diffractometer

X-ray diffraction is a common technique for study of crystal structures and atomic spacing. All X-ray diffractometers consist of three basic elements: x –ray tube, a sample holder, and x- ray detector.

X- rays generated in cathode ray tube by heating filament to produce electrons, accelerating the electrons toward a target by applying a voltage, and bombarding the a target material with electrons. When electrons have sufficient energy to dislodge inner shell electrons of target material, characteristic x- ray spectra are produced. These spectra consist of several components, the most common beingk_{α} andk_{β}. k_{α} Consist in part of $k_{\alpha 1}$ and$k_{\alpha 2}$. $k_{\alpha 1}$has slightly shorter wavelength and twice the intensity as Kα2. The specific wavelengths are characteristic of the target material (Cu, Fe, Mo, and Cr). Filtering, by foils or crystal monochrometers, is required to produce monochromatic X-rays needed for diffraction. Kα1and Kα2 are sufficiently close in wavelength such that a weighted average of the two is used. Copper is the most common target material for single-crystal diffraction, with Cu Kα radiation = 1.5418Å. These X-rays are collimated and directed onto the sample. As the sample and detector are rotated, the intensity of the reflected X-rays is recorded. When the geometry of the incident X-rays impinging the sample satisfies the Bragg Equation, constructive interference occurs and a peak in intensity occurs. A detector records and processes this X-ray

signal and converts the signal to a count rate which is then output to a device such as a printer or computer monitor [28].

Figure (4.5): X-Ray diffract meter: XRD (wavelength 1.54 A°).

4.4.2FTIR Spectroscopy

FTIR spectroscopy is a widely used technique for investigating materials. It is based on the interaction electromagnetic radiation and natural vibration of chemical bonds among atoms that compose the matter.

The main components of FTIR spectroscopy are: IR source, Michelson interferometer and IR detector. The more stable source of radiation, emitting in the three IR regions is the Ever-Glo ceramic. By using the appropriate beam splitter (interferometer components) and IR detector in combination with this source, it is possible to provide energy for the spectral range from to. The Michelson interferometer basically consists of two perpendicularly plane mirrors (one is fixed and the other movable) and beam splitter. The function of an interferometer is split

beam of light into two beams and to introduce an optical path difference between them. As a consequence, the path difference creates the condition for that interference to take place when the beams recombine at the beam splitter. The intensity vibrations of the beam emerging from the interferometer are monitored as function of path difference by the detector. The light intensity versus the optical path difference is called an interferogram. The Fourier-transform is mathematic tool used to convert the interferogram into spectrum, which is done by computer [89, 90].

Figure (4.6): FTIR (Mattson, model 960m0016) spectroscopy.

4.4.3 Ultraviolet -Visible Spectroscopy (UV-Visible)

Ultraviolet and Visible Spectroscopy is absorption spectroscopy uses electromagnetic radiations between 190 nm to 800 nm and is divided into the ultraviolet (UV, 190-400 nm) and visible (VIS, 400-800 nm) regions. Since the absorption of ultraviolet or visible radiation by a molecule leads transition among electronic energy levels of the molecule, it is also often called as electronic spectroscopy [82].When radiation interacts with matter, a number of processes can occur, including reflection, scattering, absorbance, Fluorescence/phosphorescence (absorption and reemission), and photochemical reaction (absorbance and bond breaking). In general, when measuring UV-visible spectra, we want only absorbance to occur. Because light is a form of energy, absorption of light by matter causes the energy content of the molecules (or atoms) to increase. The total potential energy of a molecule generally is represented as the sum of its electronic, vibrational, and rotational energies [91, 92].

The absorption spectra of prepared nanoparticles were measured using shimadzu spectrophotometer (UV mini 1240) in 190-800nm range see figure (3.2)

Figure (4.7): UV mini 1240 spectrometer shimadzu.

Chapter Five

Results and Discussion

5.1 Introduction

In this part of research, the main results that have been obtained from the experiments made of ($Ba_x Fe_{(1-x)} TiO_4$) (x=1, 0.1, 0.2, 0.3, 0.5, 0.6, 0.7,08, 0.9 and 0) Molar where Nanomaterials are presented. The data of X-ray diffraction (XRD) have been analyzed by using Rietveld method to ensure good quality of the samples by determined their (crystal structure, lattice parameters, the positions of atoms within the cell). The data of UV-visible used to evaluate the band gap and optical properties. The electrical and magnetic properties calculated from optical method.

5.2 X-ray Diffraction (XRD) Results of ($Ba_x Fe_{(1-x)} TiO_4$) Samples

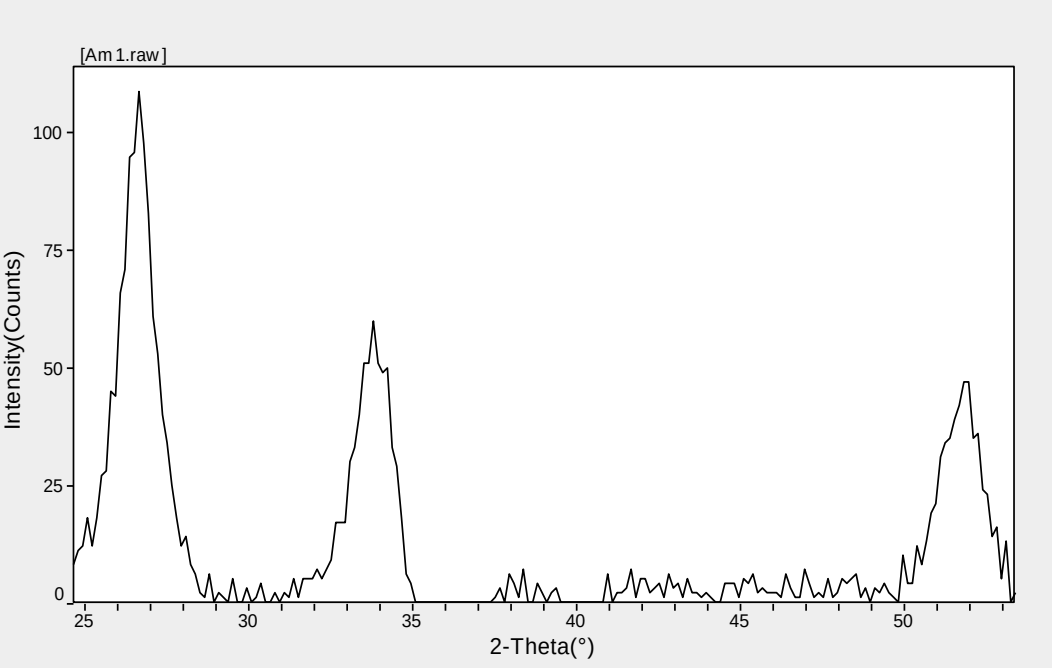

Figure (5.1): XRD spectrum of $Ba_{1.0} Fe_{0.0} Ti O_4$ sample.

Table (5.1): Calculate Lattice Constants from Peak Locations and Miller Indices [Tetragonal – primitive] of $Ba_{1.0}$ Fe $_{0.0}$ Ti O_4 sample

2Θ (^{O})	d (A^O)	h l k	X_s (nm)
26.630	3.3443	1 1 2	14.0
33.796	2.6501	1 0 1	11.8
51.794	1.7637	2 1 1	12.1

Crystal form is tetragonal primitive

Space group =P42/mm (136)

Lattice parameter: a= b= 4.7033, c =3.3056 and $\beta = \alpha = \gamma = 90^O$

Cell volume= ($73.1A^O$) 2

Density = 4.2635 $mg.cm^{-3}$

Average lattice constant = 4.7282

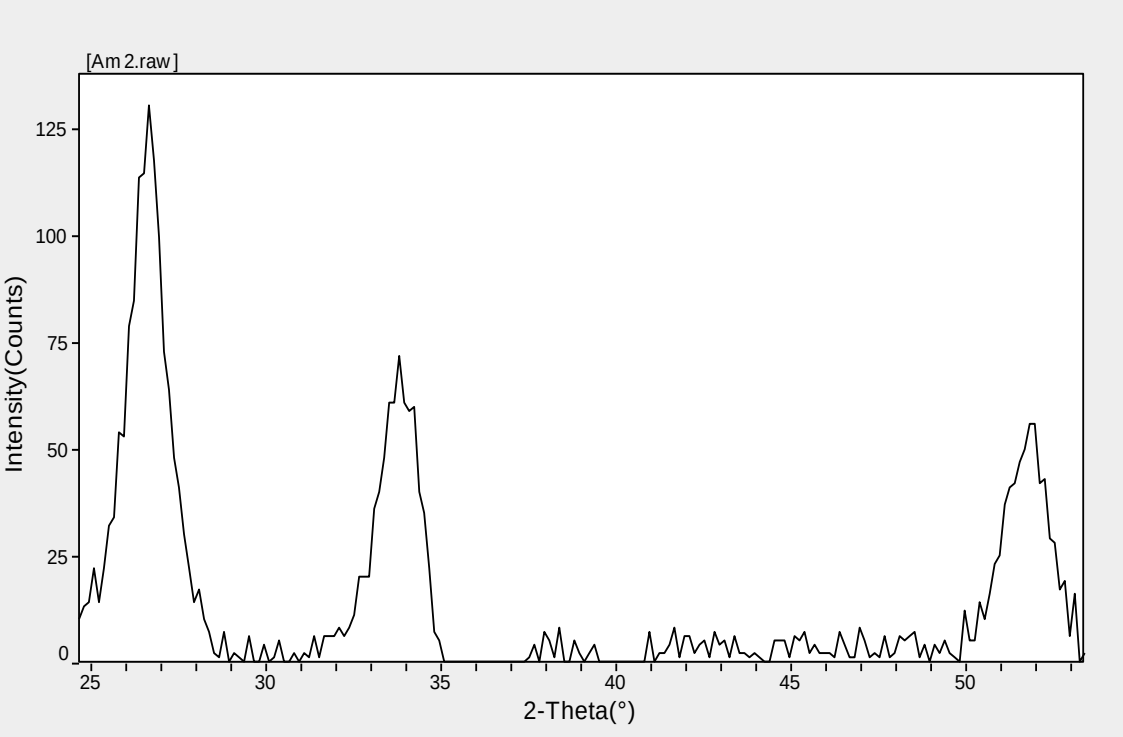

Figure (5.2): XRD spectrum of $Ba_{0.1}$ Fe $_{0.9}$ Ti O_4 sample.

Table (5.2): Calculate Lattice Constants from Peak Locations and Miller Indices [Tetragonal – primitive] of $Ba_{0.1}$ Fe $_{0.9}$ Ti O_4 sample

2Θ (^{O})	d (A^{O})	h l k	X_s (nm)
26.630	3.3441	1 1 2	14.0
33.796	2.6502	1 0 1	11.7
51.794	1.7636	2 1 1	11.4

Crystal form is tetragonal primitive

Space group =P42/mm (136)

Lattice parameter: a= b= 4.7033, c =3.3056 and $\beta = \alpha = \gamma = 90^{O}$

Cell volume= $(73.1A^{O})^{2}$

Density = 4.2635 $mg.cm^{-3}$

Average lattice constant = 4.7275

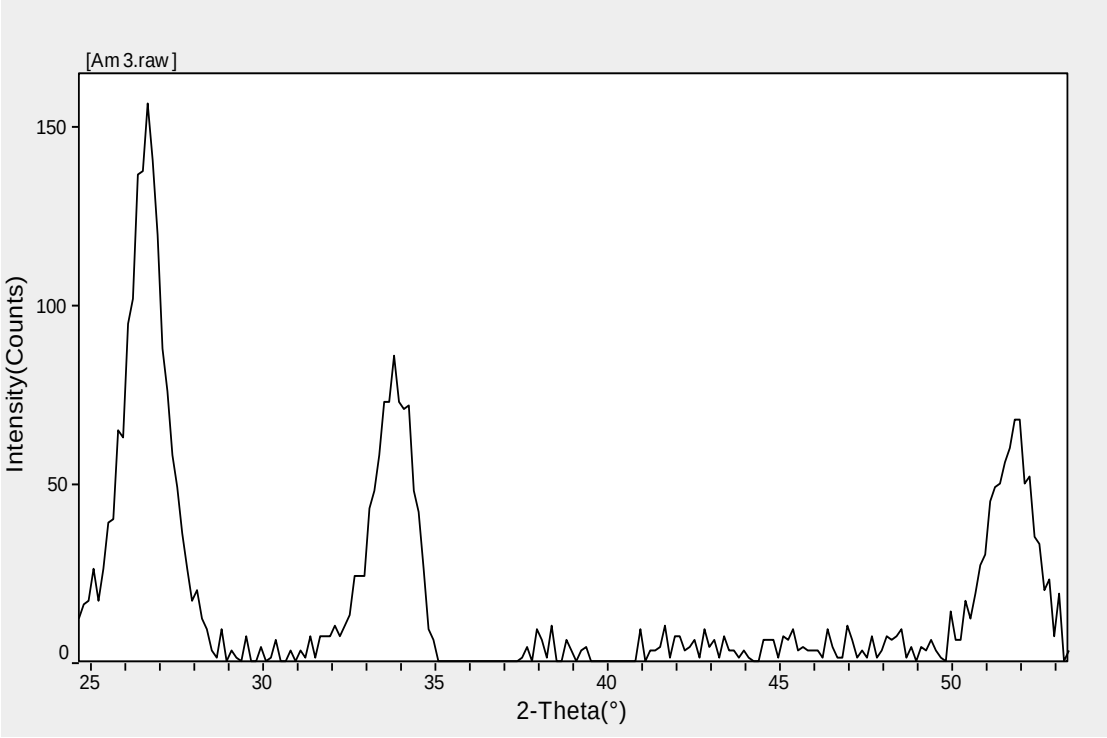

Figure (5.3): XRD spectrum of $Ba_{0.2}$ Fe $_{0.8}$ Ti O_4 sample.

Table (5.3): Calculate Lattice Constants from Peak Locations and Miller Indices [Tetragonal – primitive] of $Ba_{0.2}$ Fe $_{0.8}$ Ti O_4 sample

2Θ (^{O})	d (A^O)	h l k	X_s (nm)
26.63	3.3442	1 1 2	14.1
33.796	2.6499	1 0 1	11.5
51.794	1.7635	2 1 1	11.7

Crystal form is tetragonal primitive

Space group =P42/mm (136)

Lattice parameter: a= b= 4.7033, c =3.3056 and $\beta = \alpha = \gamma = 90^O$

Cell volume= $(73.1A^O)^2$

Density = 4.2635 mg.cm $^{-3}$

Average lattice constant = 4.7273.

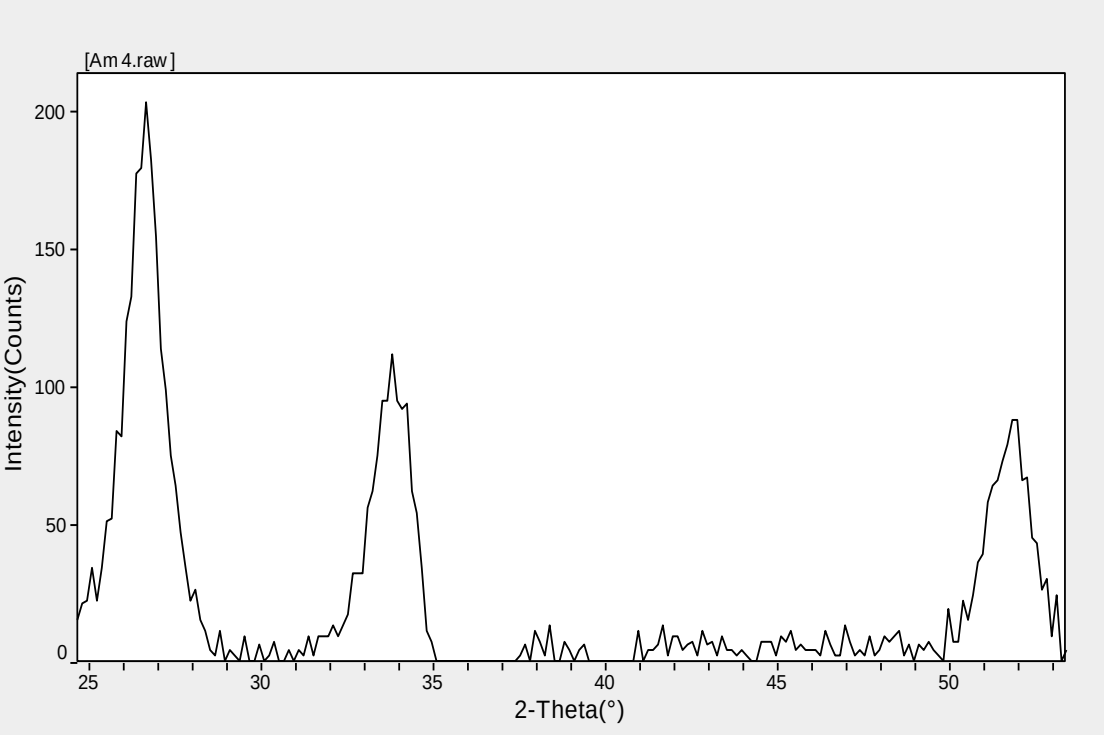

Figure (5.4): XRD spectrum of $Ba_{0.3}$ Fe $_{0.7}$ Ti O_4 sample.

Table (5.4): Calculate Lattice Constants from Peak Locations and Miller Indices [Tetragonal – primitive] of $Ba_{0.3}$ Fe $_{0.7}$ Ti O_4 sample

2Θ (^{O})	d (A^{O})	h l k	X_s (nm)
26.630	3.3442	1 1 2	14.0
33.796	2.6499	1 0 1	11.8
51.794	1.7636	2 1 1	11.1

Crystal form is tetragonal primitive

Space group =P42/mm (136)

Lattice parameter: a= b= 4.7033, c =3.3056 and $\beta = \alpha = \gamma = 90^{O}$

Cell volume= $(73.1A^{O})^{2}$

Density = 4.2635 $mg.cm^{-3}$

Average lattice constant = 4.7273

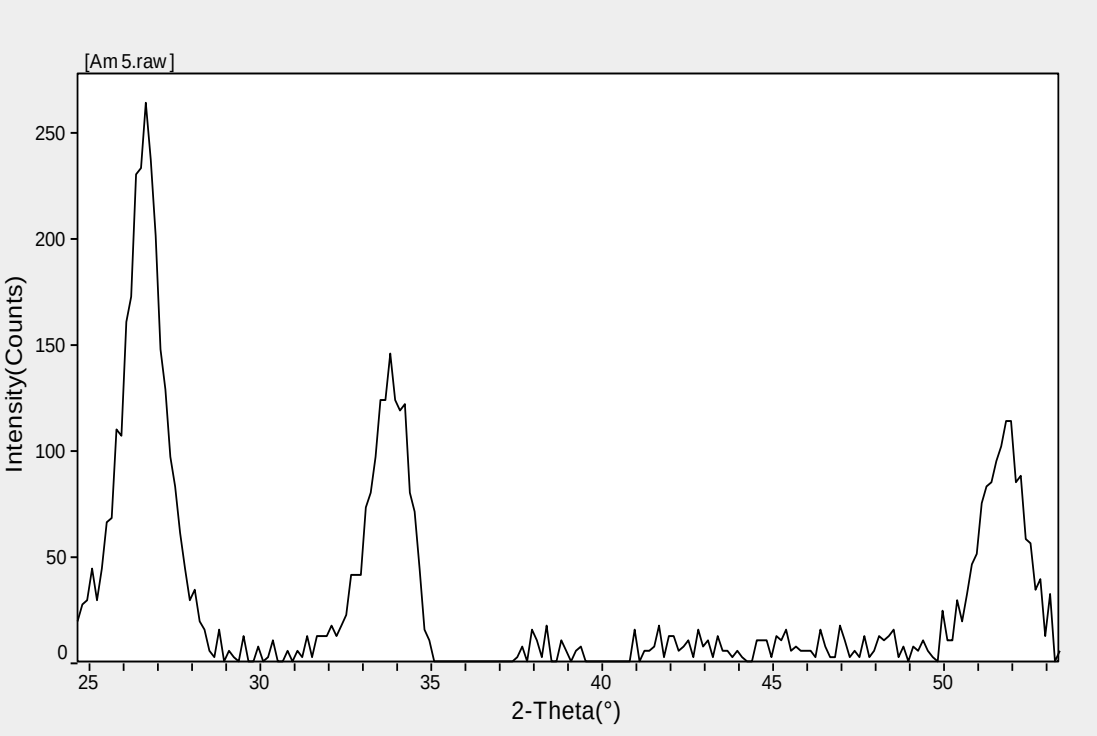

Figure (5.5): XRD spectrum of $Ba_{0.5}$ Fe $_{0.5}$ Ti O_4 sample.

Table (5.5): Calculate Lattice Constants from Peak Locations and Miller Indices [Tetragonal – primitive] of $Ba_{0.5}$ Fe $_{0.5}$ Ti O_4 sample

2Θ (^{O})	d (A^O)	h l k	X_s (nm)
26.630	3.3444	1 1 2	11.4
33.796	2.6501	1 0 1	11.7
51.794	1.7636	2 1 1	12.1

Crystal form is tetragonal primitive

Space group =P42/mm (136)

Lattice parameter: a= b= 4.7033, c =3.3056 and $\beta = \alpha = \gamma = 90^O$

Cell volume= $(73.1A^O)^2$

Density = 4.2635 $mg.cm^{-3}$

Average lattice constant = 4.7268

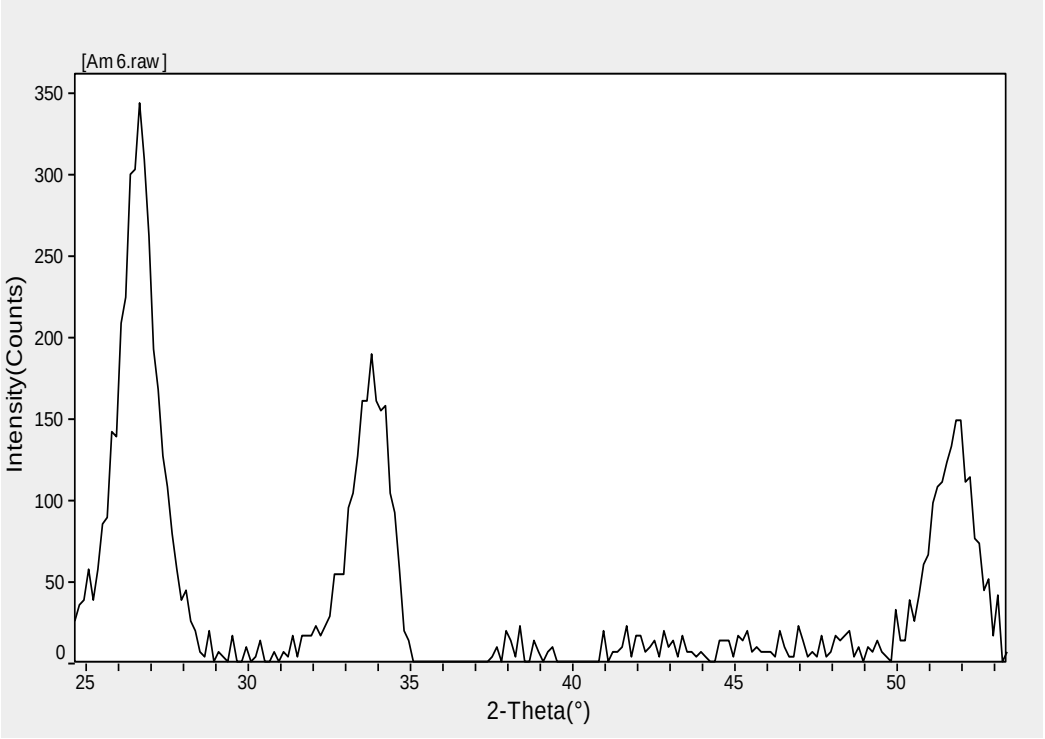

Figure (5.6): XRD spectrum of $Ba_{0.6}$ Fe $_{0.4}$ Ti O_4 sample.

Table (5.6): Calculate Lattice Constants from Peak Locations and Miller Indices [Tetragonal – primitive] of $Ba_{0.6}$ Fe $_{0.4}$ Ti O_4 sample

2Θ (^{O})	d (A^{O})	h l k	X_s (nm)
26.630	3.3430	1 1 2	10.2
33.796	2.6501	1 0 1	8.2
51.794	1.6369	2 1 1	9.7

Crystal form is tetragonal primitive

Space group =P42/mm (136)

Lattice parameter: a= b= 4.7033, c =3.3056 and $\beta = \alpha = \gamma = 90^{O}$

Cell volume= $(73.1A^{O})^{2}$

Density = 4.2635 $mg.cm^{-3}$

Average lattice constant = 4.7263

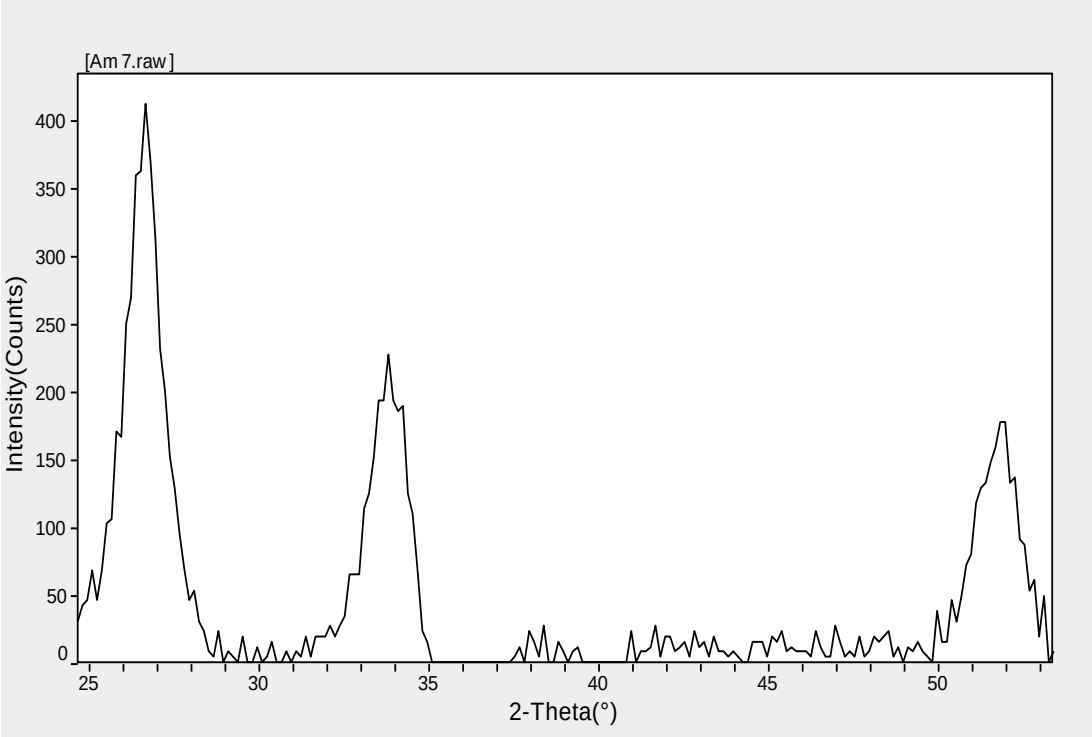

Figure (5.7): XRD spectrum of $Ba_{0.7}$ Fe $_{0.3}$ Ti O_4 sample.

Table (5.7): Calculate Lattice Constants from Peak Locations and Miller Indices [Tetragonal – primitive] of $Ba_{0.7}$ Fe $_{0.3}$ Ti O_4 sample

2Θ (^{O})	d (A^O)	h l k	X_s (nm)
26.630	3.3424	1 1 2	11.4
33.796	2.6501	1 0 1	11.7
51.794	1.6372	2 1 1	9.2

Crystal form is tetragonal primitive

Space group =P42/mm (136)

Lattice parameter: a= b= 4.7033, c =3.3056 and $\beta = \alpha = \gamma = 90^O$

Cell volume= $(73.1A^O)^2$

Density = 4.2635 $mg.cm^{-3}$

Average lattice constant = 4.7261

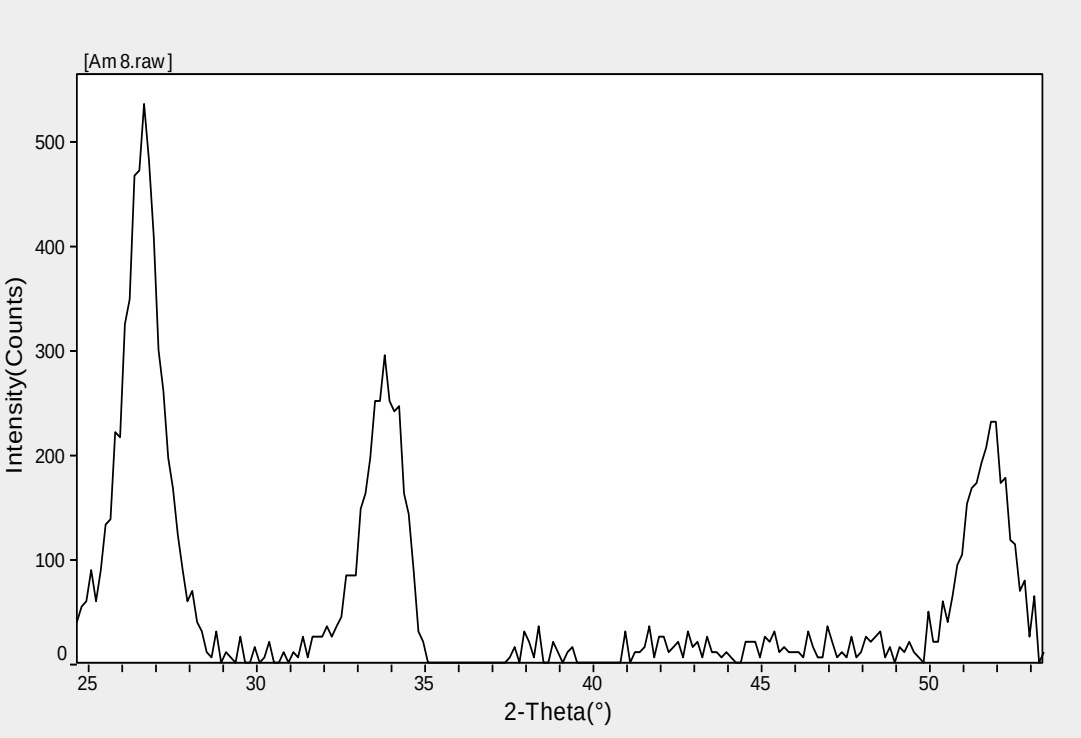

Figure (5.8): XRD spectrum of $Ba_{0.8}$ Fe $_{0.2}$ Ti O_4 sample.

Table (5.8): Calculate Lattice Constants from Peak Locations and Miller Indices [Tetragonal – primitive] of $Ba_{0.8}$ Fe $_{0.2}$ Ti O_4 sample

2Θ (^{O})	d (A^{O})	h l k	X_s (nm)
26.630	3.349	1 1 2	11.3
33.796	2.6501	1 0 1	11.6
51.794	1.6374	2 1 1	8.9

Crystal form is tetragonal primitive

Space group =P42/mm (136)

Lattice parameter: a= b= 4.7033, c =3.3056 and $\beta = \alpha = \gamma = 90^{O}$

Cell volume= $(73.1A^{O})^{2}$

Density = 4.2635 $mg.cm^{-3}$

Average lattice constant = 4.7260

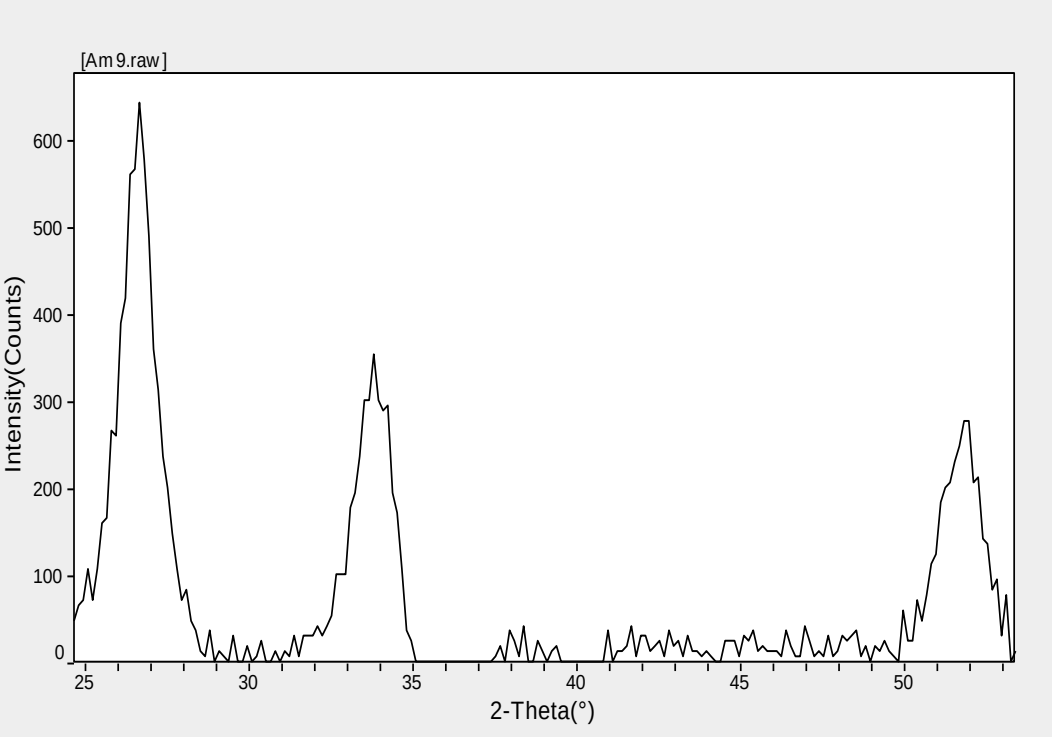

Figure (5.9): XRD spectrum of $Ba_{0.9}$ Fe $_{0.1}$ Ti O_4 sample.

Table (5.9): Calculate Lattice Constants from Peak Locations and Miller Indices [Tetragonal – primitive] of $Ba_{0.9}$ Fe $_{0.1}$ Ti O_4 sample

2Θ (^{O})	d (A^O)	h l k	X_s (nm)
26.630	3.3445	1 1 2	12.1
33.796	2.6501	1 0 1	11.7
51.794	1.7634	2 1 1	11.7

Crystal form is tetragonal primitive

Space group =P42/mm (136)

Lattice parameter: a= b= 4.7033, c =3.3056 and $\beta = \alpha = \gamma = 90^O$

Cell volume= $(73.1A^O)^2$

Density = 4.2635 $mg.cm^{-3}$

Average lattice constant = 4.7256

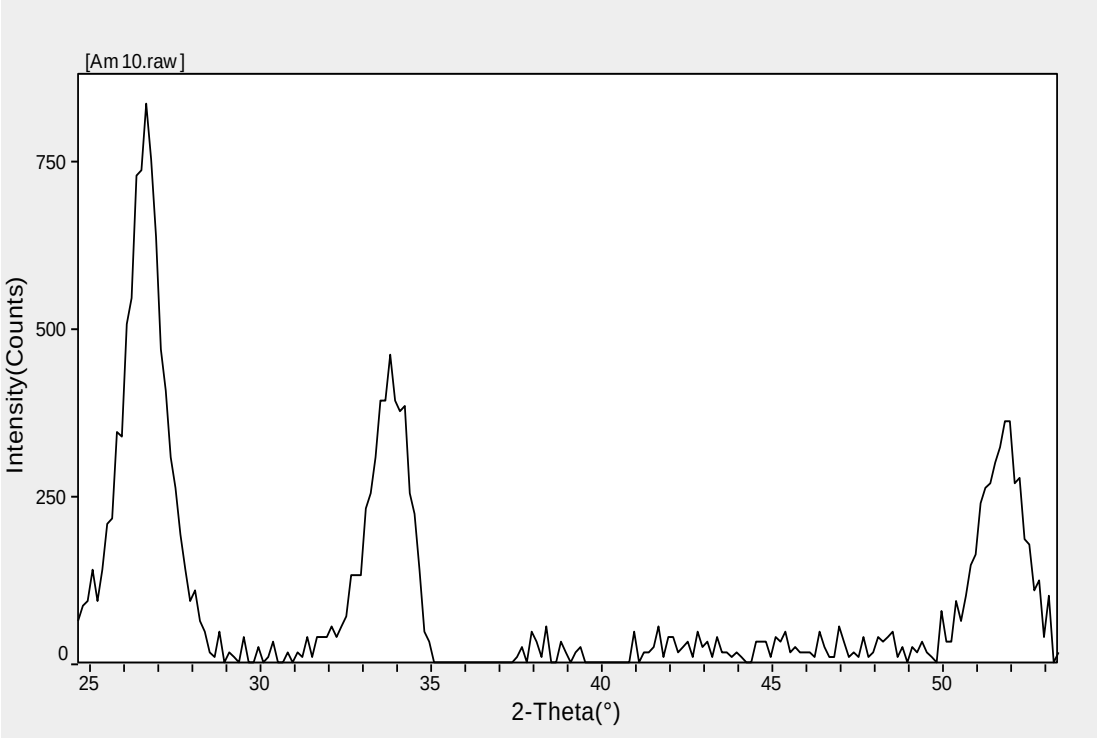

Figure (5.10): XRD spectrum of $Ba_{0.0}$ Fe $_{1.0}$ Ti O_4 sample.

Table (5.10): Calculate Lattice Constants from Peak Locations and Miller Indices [Tetragonal – primitive] of $Ba_{0.0}$ Fe $_{1.0}$ Ti O_4 Sample

2Θ (^{O})	d (A^O)	h l k	X_s (nm)
26.630	3.3445	1 1 2	12.0
33.796	2.6501	1 0 1	11.6
51.794	1.7636	2 1 1	12.0

Crystal form is tetragonal primitive

Space group =P42/mm (136)

Lattice parameter: a= b= 4.7033, c =3.3056 and $\beta = \alpha = \gamma = 90^O$

Cell volume= (73.1A^{O}) 2

Density = 4.2635 mg.cm $^{-3}$

Average lattice constant = 4.6104

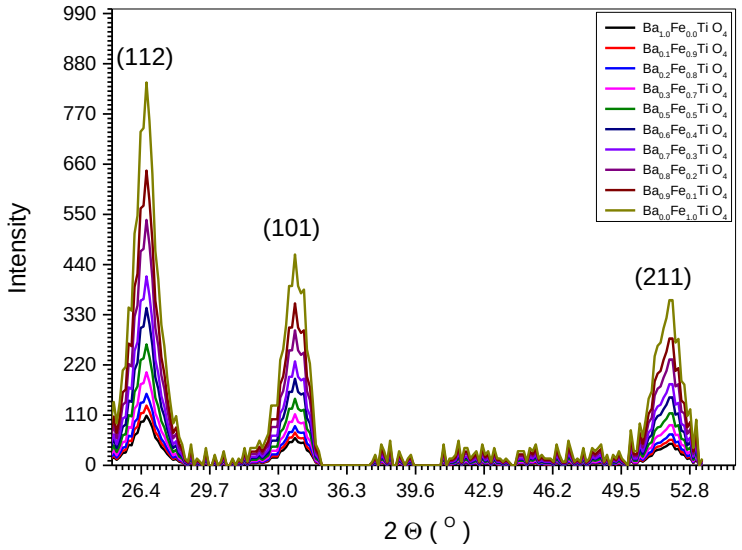

Figure (5.11): XRD spectrum of all ($Ba_x Fe_{(1-x)} TiO_4$) samples.

Table (5.11): Some Crystallite Lattice Parameter, Average Lattice Constant ,Xs(nm) and d – Spacing) of ($Ba_x Fe_{(1-x)} TiO_4$) Samples

Sample	**a=b**	**C**	**α=β = γ**	**Average Lattices constant**	**Xs(nm)**	**d-Spacing**
$Ba_{1.0}Fe_{0.0}TiO_4$	4.7033	3.3056	90	4.7282	12.6	2.5861
$Ba_{0.1}Fe_{0.9}TiO_4$	4.7033	3.3056	90	4.7275	12.4	2.5860
$Ba_{0.2}Fe_{0.8}TiO_4$	4.7033	3.3056	90	4.7273	12.4	2.5859
$Ba_{0.3}Fe_{0.7}TiO_4$	4.7033	3.3056	90	4.7273	12.3	2.5858
$Ba_{0.5}Fe_{0.5}TiO_4$	4.7033	3.3056	90	4.7268	11.9	2.5856
$Ba_{0.6}Fe_{0.4}TiO_4$	4.7033	3.3056	90	4.7263	11.8	2.5455
$Ba_{0.7}Fe_{0.3}TiO_4$	4.7033	3.3056	90	4.7261	11.7	2.5433
$Ba_{0.8}Fe_{0.2}TiO_4$	4.7033	3.3056	90	4.7260	10.8	2.5432
$Ba_{0.9}Fe_{0.1}TiO_4$	4.7033	3.3056	90	4.7256	10.6	2.5431
$Ba_{00}Fe_{1.0}TiO_4$	4.7033	3.3056	90	4.6104	9.4	2.5430

5.3 FTIR Results of ($Ba_x Fe_{(1-x)} TiO_4$) Samples

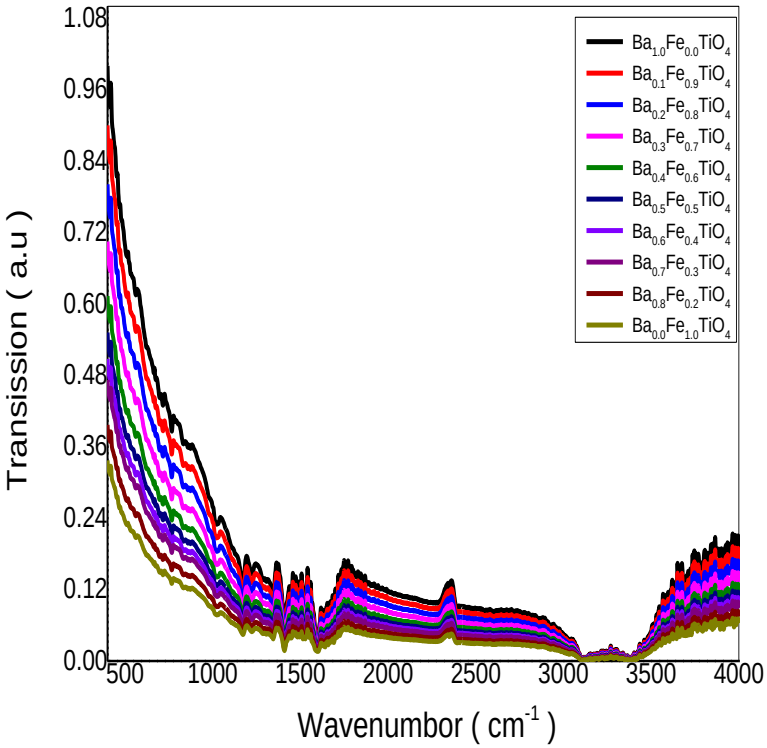

Figure (5.12): FTIR spectrum of all ($Ba_x Fe_{(1-x)} TiO_4$) samples.

Table (5.12): Illustrate IR Spectral Region (cm^{-1}), Functional Groups and Vibration Type of all ($Ba_x Fe_{(1-x)} TiO_4$) Samples

Spectral Region(cm^{-1})	Functional Group	Vibration Classification
760	Aldehydes	C-H bend
1015	Esters or Ethers	C-O stretching
1170	Esters or Ethers	C-O stretching
1230	Esters or Ethers	C-O stretching
1340	nitro	N = O bending
1415	alkenes	C-H bending
1580	nitro	N=O stretching
3100	alkenes	C=C-H Stretch
3400	Phenols & Alcohols	O-H stretching

The infrared spectra of synthesized (Ba x Fe(1-x) Ti O4) (1, 0.1 ,0.2 ,0.3 ,0.5 ,0.6, 0.7,08 ,0.9 and 0) Molar nano powders were recorded by mattson Fourier Transform Infrared Spectrophotometer in the range of 400 to 4000 cm^{-1} The spectra of all the samples have been used to locate the band positions which are given in the Table (5.12) . In the present study the absorption bands υ_1 , υ_2 , υ_3 , υ_4, υ_5, υ_6 , υ_7 ,υ_8 and $\upsilon_9$are found to be around 760 cm^{-1}, 1015cm^{-1}, 1170cm^{-1}, 1230cm^{-1}, 1340$cm^{-1}$and 1415cm^{-1}, 1580, cm^{-1}, 3100 cm^{-1}, 3400 cm^{-1}respectively for all the compositions. Then their function group and vibration mode were classified from spectroscopy data tables and listed in table (5.12)[1]. The variations of wave number as a function of transission are shown in fig. (5.12) for ten samples of ($Ba_x Fe_{(1-x)} TiO_4$) (1, 0.1 ,0.2 ,0.3 ,0.5 ,0.6, 0.7,08 ,0.9 and 0)

Molar. In figure(5.12) observed that absorption was increased as wave number was increase, the maximum value around 3400cm^{-1}.associated with the Phenols and Alcohols O-H stretching vibration. As known the transission is inversily propotional to absorption, the photon with high wave number high energy absorption $E = hc\upsilon$, where h is Plancks constant. It was noted that the maximum absorption band at wave number 3400 $cm^{-1}$is due to O-H bond. Because electronegativity which is measure of the tendency of atom to attract electrons towards itself. That for oxygen (3.44) is greater than those for nitrogen (3.04) and carbon (2.55). We can be observed the absorption increased as Fe doping increased. This implies

5.4 Optical Results of ($Ba_x Fe_{(1-x)} TiO_4$) Samples

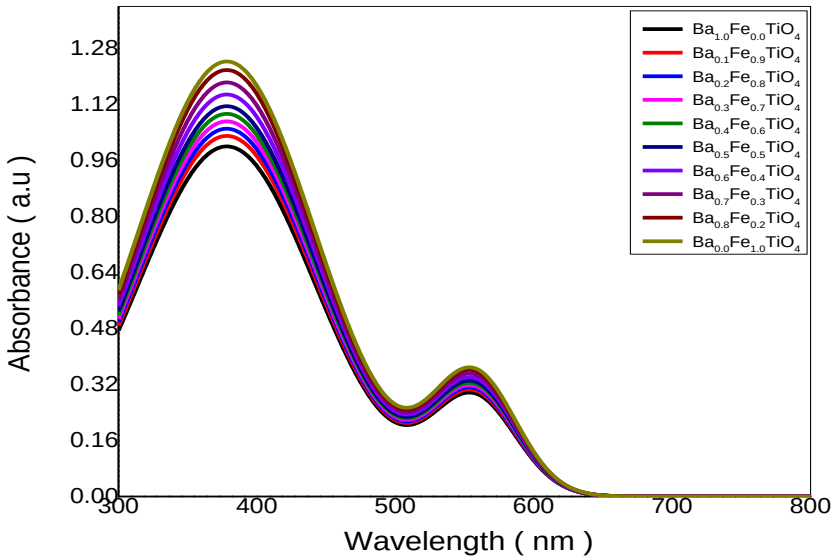

Figure (5.13): Absorbance spectrum of all ($Ba_x Fe_{(1-x)} TiO_4$) samples.

Absorbance: UV-VS min 1240 spectrophotometer was used to study the absorbance of ten samples prepered of ($Ba_x Fe_{(1-x)} TiO_4$) (1, 0.1 ,0.2 ,0.3 ,0.5 ,0.6, 0.7,08 ,0.9 and 0) Molar. Show all resolute of absorbance in fig (5.13). fig. (5.13), reveals that the behavior of curve is the same for all ten samples. also we found the relation between absorbance and wavelengths for ten samples of ($Ba_x Fe_{(1-x)} TiO_4$) (1, 0.1 ,0.2 ,0.3 ,0.5 ,0.6, 0.7,08 ,0.9 and 0) Molar , the rapid increase of the a absorption at wavelengths 380 nm crosponding photon energy 3.26 eV and at 560 nm crosponding photon energy 2.21 eV when increase Fe doping .

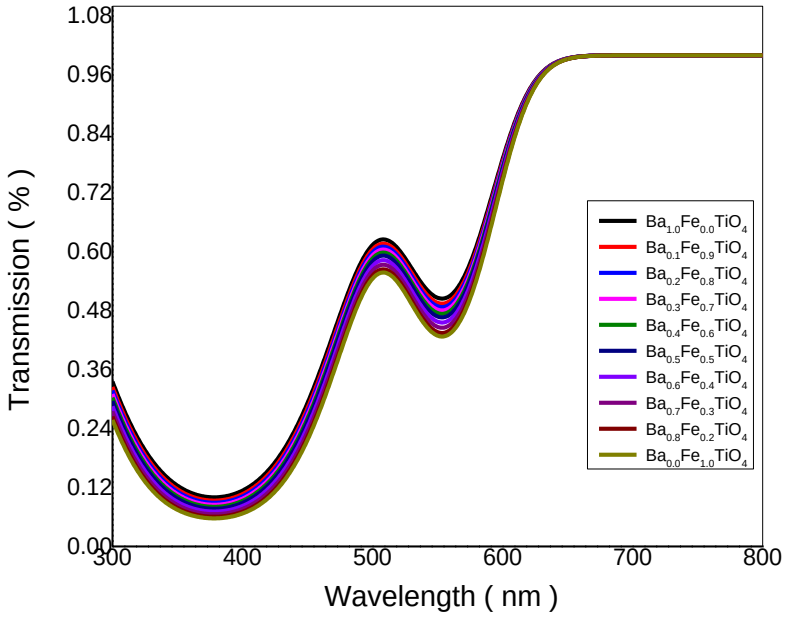

Figure (5.14): Transmission spectrum of all ($Ba_x Fe_{(1-x)} TiO_4$) samples.

Transmission Spectra: figure (5.14) shows the relation between transission and wavelengths for ten samples of ($Ba_x Fe_{(1-x)} TiO_4$) (1, 0.1, 0.2, 0.3, 0.5, 0.6, 0.7,08, 0.9 and 0) Molar. we found the behavior of curves is the same for ten samples. It

was observed the transmittance decreased with increase molar concerntration of iron(Fe). This implies doping introduces free electrons into structure of samples which absorb more amount of visable light.

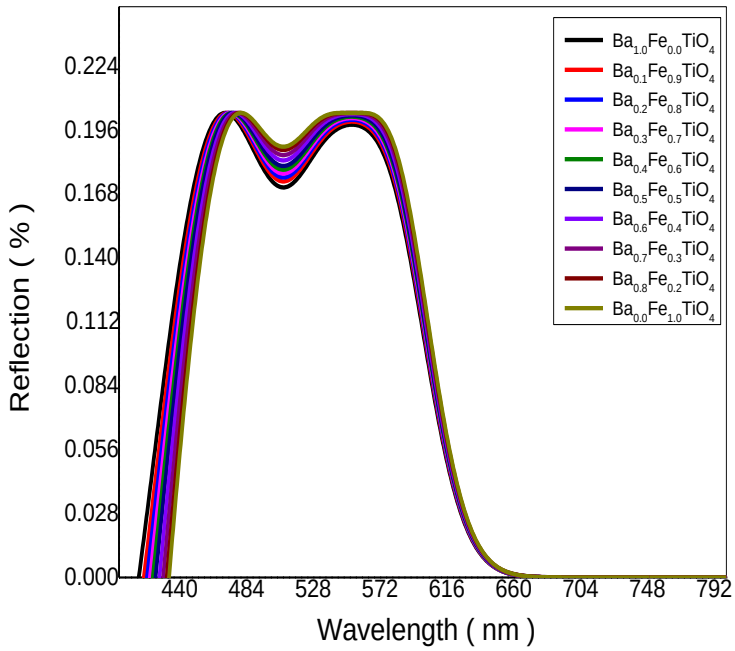

Figure (5.15): Reflection spectrum of all ($Ba_x Fe_{(1-x)} TiO_4$) samples.

Reflection Spectra: The reflection of ten samples of ($Ba_x Fe_{(1-x)} TiO_4$) (1, 0.1, 0.2, 0.3, 0.5, 0.6, 0.7,08, 0.9 and 0) Molar was shown in fig (5.15). In fig. (5.15) observed that the reflection for ten samples ($Ba_x Fe_{(1-x)} TiO_4$) had maximum value in two area the first one was ranged at (465 to 485) nm the second at (535 to 570) nm in this two point the samples become mirrors. The efficet of Fe doping on the

refelection was increase doping. the reflection was red sheft in first point and increase reflection value in the second point .

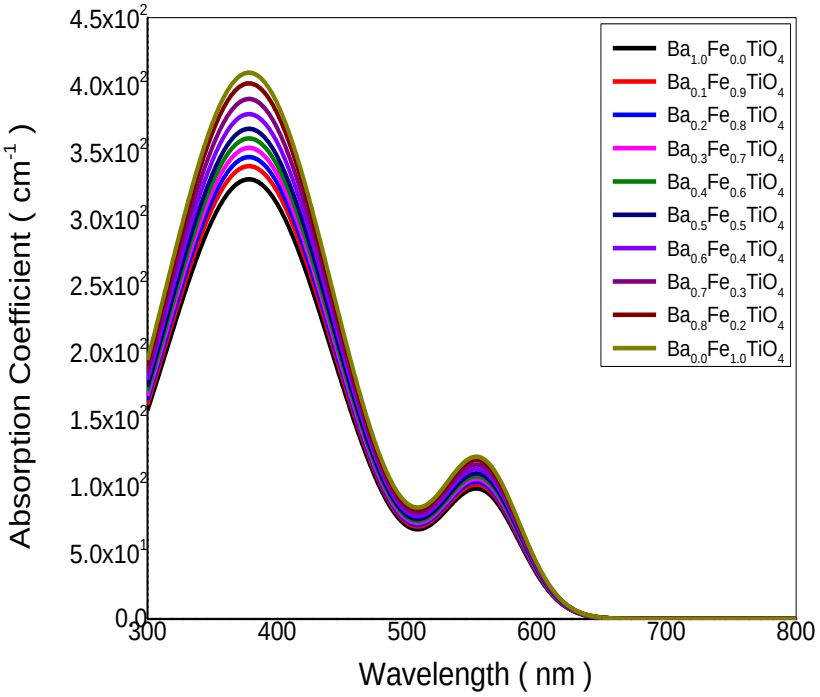

Figure (5.16): Absorption coefficient spectrum of all ($Ba_x Fe_{(1-x)} TiO_4$) samples.

Absorption Coefficient (α): figure (5.16) shows the plot of absorption Coefficient (α) with wavelength (λ) of ten samples were prepared by ($Ba_x Fe_{(1-x)} TiO_4$) (1, 0.1 ,0.2 ,0.3 ,0.5 ,0.6, 0.7,08 ,0.9 and 0) Molar. The absorption coefficient (α) of the ten prepared were determined by the following relation $\alpha = \frac{2.303xA}{t}$ where (A) is the absorbance and (t) is the optical legth in the samples. It was obtained two peaks for all samples the values of $\alpha = 4.09x10^2$ cm^{-1} at 380 nm and $1.22x10^2 cm^{-1}$ at

560 nm for $Ba_{1.0}Fe_{0.0}TiO_4$ sample, while for $Ba_{0.0}Fe_{1.0}TiO_4$ sample equal $3.28x10^2$ cm^{-1} at 380 nm , and $0.97x10^2$ cm^{-1} at 560 nm , this means that the transition must corresponding to a indirect electronic transition, and the properties of this state are important since they are responsible for electrical conduction.). We found that the values of the absorption coefficient (α) for $Ba_{1.0}Fe_{0.0}TiO_4$ sample is larger than that for $Ba_{0.0}Fe_{1.0}TiO_4$ sample as resuslt of decrease Fe doping.

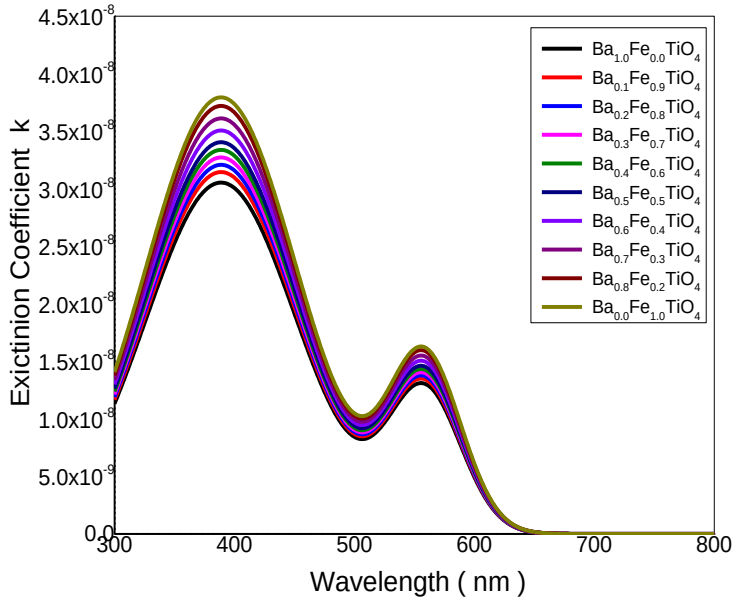

Figure (5.17): Excitation coefficient spectrum of all ($Ba_x Fe_{(1-x)} TiO_4$) samples.

Extinction Coefficient (K): Extinction coefficient (K) was calculated using the relation $k = \frac{\alpha\lambda}{4\pi}$ The variation at the (K) values as a function of (λ) are shown in fig. (5.17) for ten samples of ($Ba_x Fe_{(1-x)} TiO_4$) (1, 0.1 ,0.2 ,0.3 ,0.5 ,0.6, 0.7,08 ,0.9

and 0) Molar and we observed that the spectrum shape of (K) as the same shape of (α) because the extinction coefficient is directly proportional to absorption coefficient (α) as relation above. The Extinction coefficient (K) for ten samples of ($Ba_x Fe_{(1-x)} TiO_4$) (1, 0.1 ,0.2 ,0.3 ,0.5 ,0.6, 0.7,08 ,0.9 and 0) Molar in fig.(5.17) obtained the value of (K) at the (380 and 560) nm wavelength was depend on the samples treatment method. We found the value of (K) at the wavelength 380 nm equal equal $3.79x10^{-8}$for $Ba_{0.0}Fe_{1.0}TiO_4$ sample while for other sample $Ba_{1.0}Fe_{0.0}TiO_4$ equal $3.05x10^{-8}$, and at the wavelength 560 nm for $Ba_{0.0}Fe_{1.0}TiO_4$ sample equal $1.65x10^{-8}$ while for other sample $Ba_{1.0}Fe_{0.0}TiO_4$ equal $1.31x10^{-8}$ .The efficet of Fe doping on the Extinction coefficient (K) was increase Fe doping decrease the Extinction coefficient (K)

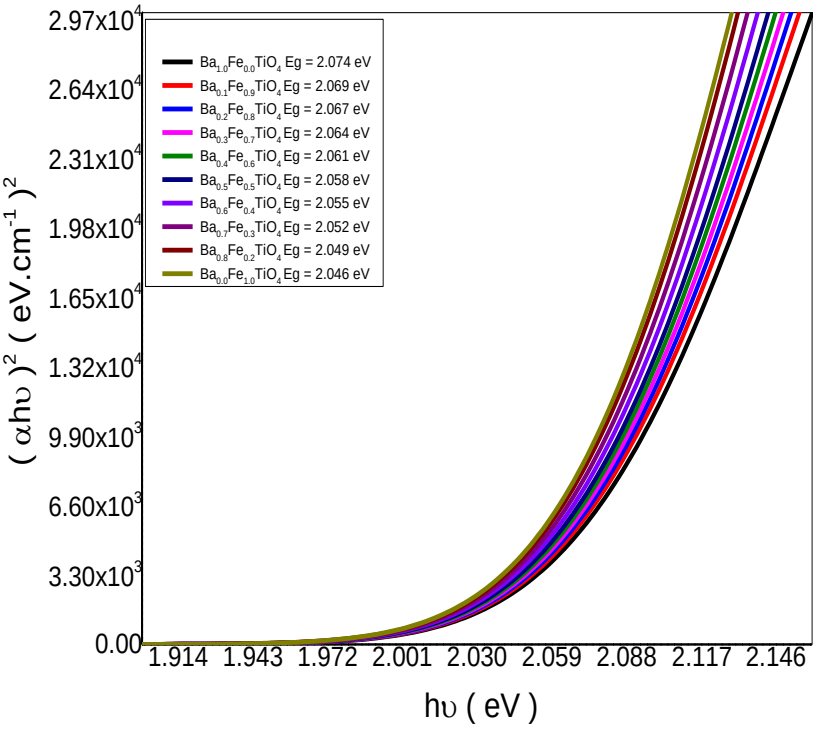

Figure (5.18): Optical energy band gap spectrum of all ($Ba_x Fe_{(1-x)} TiO_4$) samples.

The Optical Energy Gap (Eg): The optical energy gap (Eg) has been calculated by the relation $(\alpha h\upsilon)^2 = C(h\upsilon - Eg)$ where (C) is constant, by plotting $(\alpha h\upsilon)2$ vs photon energy ($h\upsilon$) as shown in fig.(5.18) for the ten samples prepared by ($Ba_x Fe_{(1-x)} TiO_4$) (1, 0.1 ,0.2 ,0.3 ,0.5 ,0.6, 0.7,08 ,0.9 and 0) Molar . And by extrapolating the straight thin portion of the curve to intercept the energy axis , the value of the energy gap has been calculated,as flowing for $Ba_{1.0}Fe_{0.0}TiO_4$ sample the value of (Eg) obtained was (2.046) eV while for other sample $Ba_{0.0}Fe_{1.0}TiO_4$ obtained was (2.074) eV. It was observed that the value of(Eg) was decreased from (2.074) eV to (2.046) eV. Figure (2), indicates that upon decreasing Fe concentration decrease the energy gap.

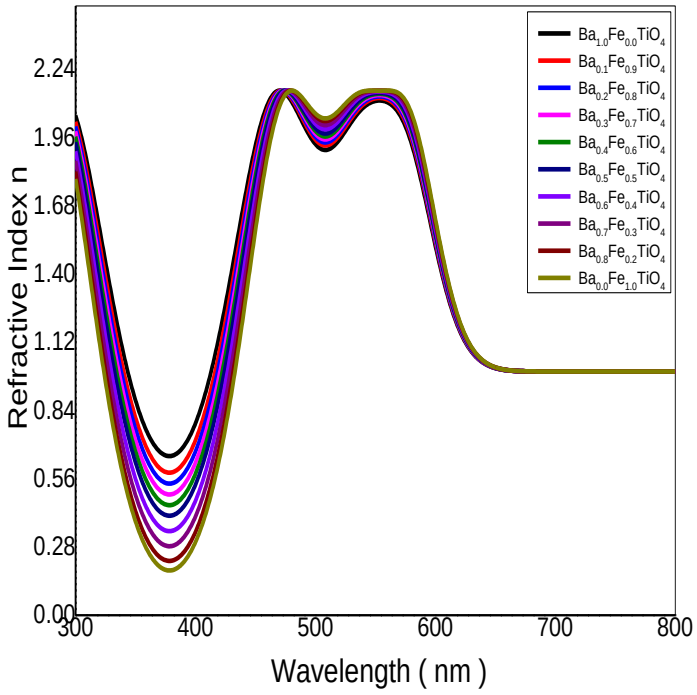

Figure (5.19): Refractive index spectrum of all ($Ba_x Fe_{(1-x)} TiO_4$) samples.

The Refractive Index (n): The refractive index (n) is the relative between speed of light in vacuum to its speed in material which does not absorb this light. The value of n was calculated from the equation $n = [\left(\frac{(1+R)}{(1-R)}\right)^2 - (1 + k^2)]^{\frac{1}{2}} + \frac{(1+R)}{(1-R)}]$ Where (R) is the reflectivity. The variation of (n) vs (λ) for ten samples was prepered by ($Ba_x Fe_{(1-x)} TiO_4$) (1, 0.1 ,0.2 ,0.3 ,0.5 ,0.6, 0.7,08 ,0.9 and 0) Molar was shown in fig.(5.19) . in fig (5.19) obseved that the maximum value of (n) is (2.166) for all samples at two area the first one in range (465 to 485) nm the second (535 to 570) nm, the first point was agreement with red shift by increase Fe on the samples , and increase the value of refractive index by increase Fe on the second point . Also we can show that the value of (n) begin to decrease befor 465 nm and after 585 nm of region spectrum . As can be observed in figure(5.19), the refractive index is increase with increase Fe doping. This behaviour can be explained on the basis increases in Fe make extra energy bands in forbiden energy band which acts refraction centre of incindent rays this cuases increase in the reflectivity so increasing in refractive index.

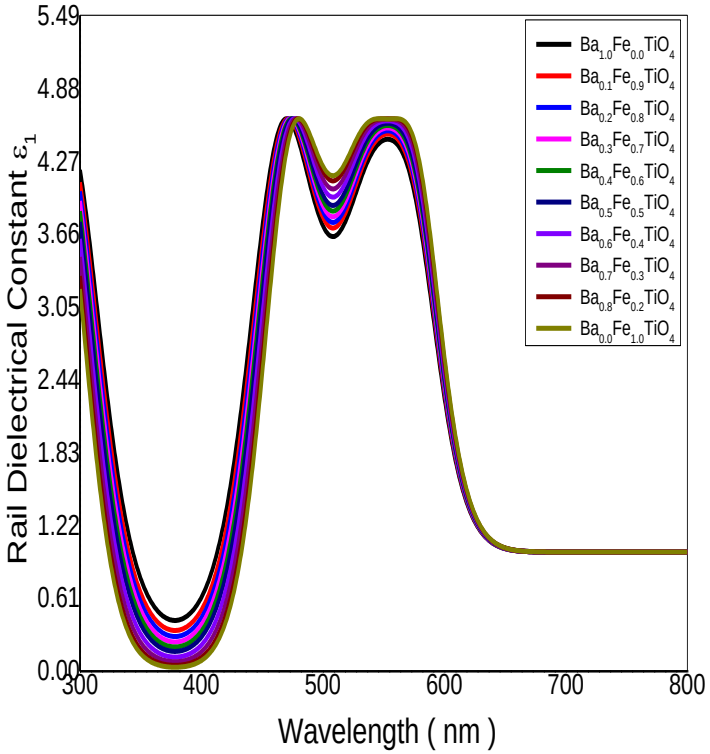

Figure (5.20): Rail dialectical constant spectrum of all ($Ba_x Fe_{(1-x)} TiO_4$) samples.

Real Dielectric Constant (ε_1) : Fig(5.20) shows the variation of the real dielectric constant (ε_1) with wavelength of ten samples prepared by ($Ba_x Fe_{(1-x)} TiO_4$) (1, 0.1 ,0.2 ,0.3 ,0.5 ,0.6, 0.7,08 ,0.9 and 0) Molar , which calculated by the relation $\varepsilon_1 = n^2 - k^2$ Where the real the dielectric (ε_1) is the normal dielectric constant, k is excintation coefficient . From fig (4.19) the variation of (ε_1) is follow the refractive index, where the maximum at two area the first one in range (465to 485) nm the second at (535to 570) nm for all samples prepered, where the absorption of the samples at these wavelength is small, but the polarization was increase. The maximum value of (ε1) is equal to (4.65) for two area. The effect of treatment by

(Ba $_x$ Fe$_{(1-x)}$ TiO$_4$) (1, 0.1 ,0.2 ,0.3 ,0.5 ,0.6, 0.7,08 ,0.9 and 0) Molar on the (ε1) was red sheft on the first point when Fe increase , But increase on the second point when Fe increase .

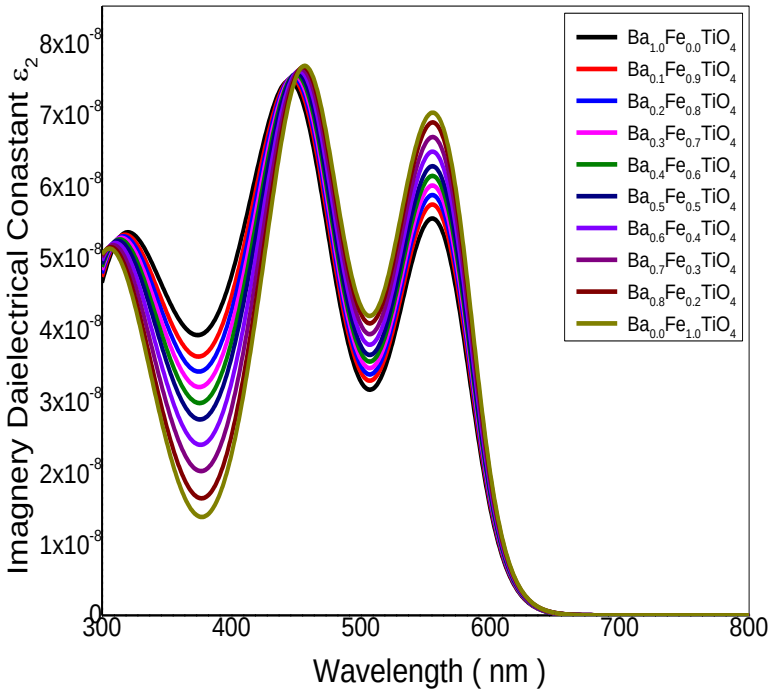

Figure (5.21): Imaginary dialectical constant spectrum of all (Ba $_x$ Fe $_{(1-x)}$ TiO$_4$) samples.

The Imaginary Dielectric Constant (ε$_2$): The imaginary dielectric constant (ε$_2$) vs (λ) was shown in fig(5.21) this value calculated from the relation ε$_2$ = 2nK (ε$_2$) represent the absorption associated with free carriers.As shown in fig(5.21) the shape of (ε$_2$)is the same as (ε$_1$), this means that the refractive index was dominated in these behavior . The maximum values of (ε$_2$) are different according to the treatment operation , so the maximum value of (ε2) equal at two area the first one equal (7.69x10^{-8}) in ranged (465 to 485) nm while the second equal (7.06x10^{-8}) in

range(535 to 570), these behavior may by related to the different absorption mechanism for free carriers.

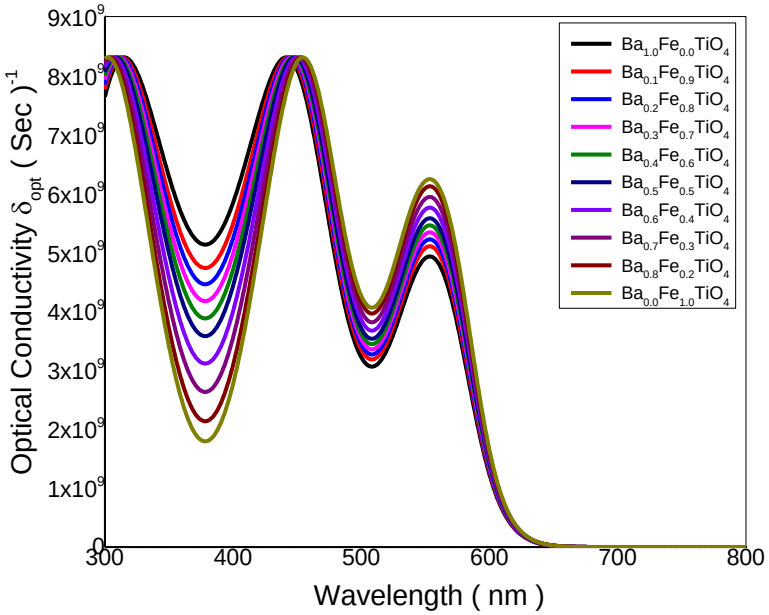

Figure (5.22): Optical conductivity spectrum of all ($Ba_x Fe_{(1-x)} TiO_4$) samples.

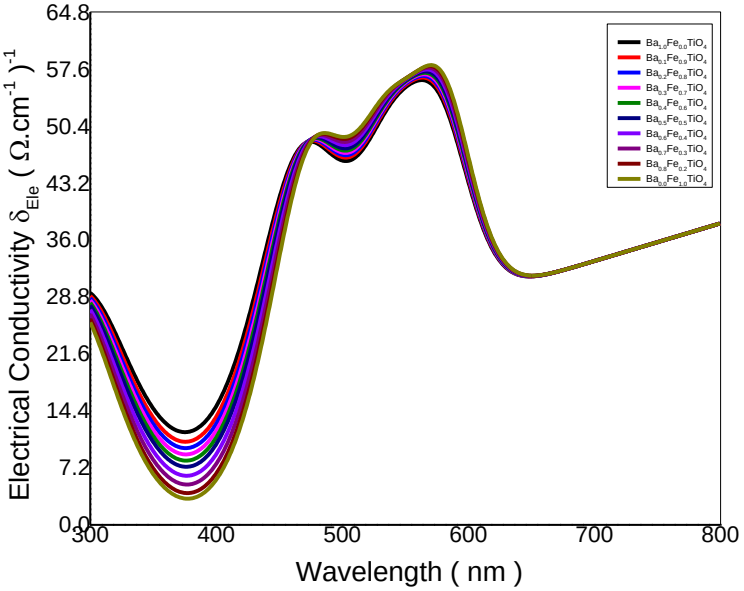

Figure (5.23): Electrical conductivity spectrum of all ($Ba_x Fe_{(1-x)} TiO_4$) samples.

Electrical and Optical Conductivity: The optical conductivity is a measure of frequency response of material when irradiated with light which is determined using the following relation, $\delta_{opt} = \frac{\alpha nc}{4\pi}$ Where (c) is the light velocity. The electrical conductivity can be estimated using the following relation $\delta_{ele} = \frac{2\lambda\delta_{opt}}{\alpha}$. The high magnitude of optical conductivity ($8.36x10^9$ sec^{-1}) confirms the presence of very high photo-response of the ten samples prepared by ($Ba_x Fe_{(1-x)} TiO_4$) (1, 0.1 ,0.2 ,0.3 ,0.5 ,0.6, 0.7,08 ,0.9 and 0) Molar . The increased of optical conductivity at high photonenergies is due to the high absorbance of ten samples prepared by ($Ba_x Fe_{(1-x)} TiO_4$) (1, 0.1 ,0.2 ,0.3 ,0.5 ,0.6, 0.7,08 ,0.9 and 0) Molar due to electron excitation by photon energy as it is shown in Figs (5.22) and (5.23) . The optical and electrical conductivities in figures (5.22) and (5.23) showincrease

of conductivity upon increasing Fe concentration for shorter wavelengths and the conductivity decreases upon increasing Fe concentration at long wavelength.

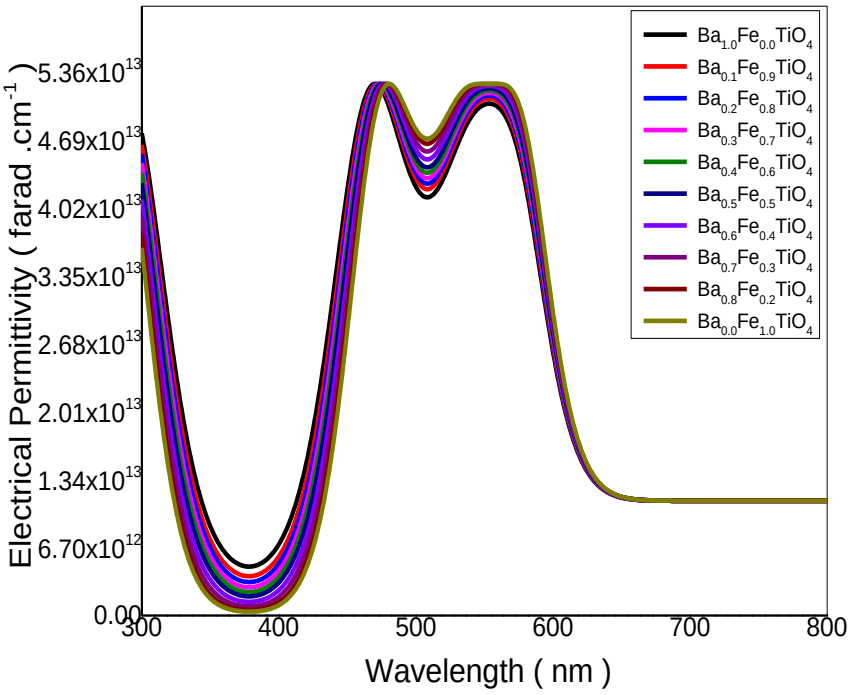

Figure (5.24): Electrical permittivity (ε_r) spectrum of all ($Ba_x Fe_{(1-x)} TiO_4$) samples.

Electrical Permittivity: The Electrical Permittivity (ε_r) spectrum of all ($Ba_x Fe_{(1-x)} TiO_4$) samples vs (λ) was shown in fig(5.24) this value calculated from the relation $\varepsilon_r = \frac{8.85x10^{-12}}{\sqrt{n}}$ where n is refractive index represent the absorption associated with free carriers .As shown in fig(5.24) the shape of (ε_r) in wavelength fuction . this means that the refractive index was dominated in these behavior . The values of (ε_r) are different according to the treatment operation , so the value of (ε_r)

equal ($2.3765x10^{13}$ farad.cm^{-1}) at (550) nm for $Ba_{0.0}Fe_{1.0}$ Ti O_4 sample while for $Ba_{1.0}Fe_{0.0}$ Ti O_4 sample equal ($2.17175x10^{13}$ frad .cm^{-1}) at the same wavelenghths, these behavior may by related to the different absorption mechanism for free carriers, and the The Electrical Permittivity (ε_r) increarse by the rate of (Fe) increases .

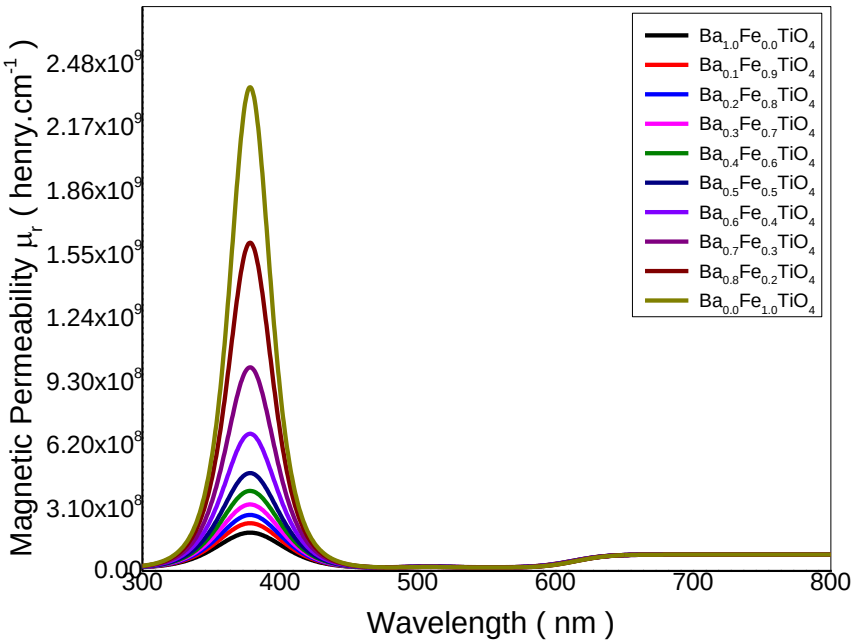

Figure (5.25): Magnetic permeability (μ_r) spectrum of all (Ba $_x$ Fe $_{(1-x)}$ TiO_4) samples.

Magnetic Permeability: The Magnetic Permeability (μ_r) spectrum of all (Ba $_x$ Fe $_{(1-x)}$ TiO_4) samples vs (λ) was shown in fig(5.25) this value calculated from the relation $\mu_r = \frac{\sqrt{n}}{1.257x10^{-6}}$ where n is refractive index represent the absorption

associated with free carriers .As shown in fig(5.25) the shape of (μ_r) in wavelength fuction . this means that the refractive index was dominated in these behavior . The values of (μ_r) are different according to the treatment operation , so the value of (μ_r)equal ($2.36x10^9$ henry $.cm^{-1}$) at (377) nm for $Ba_{0.0}Fe_{1.0}$ Ti O_4 sample while for $Ba_{1.0}Fe_{0.0}$ Ti O_4 sample equal ($1.92x10^8$ henry $.cm^{-1}$) at the same wavelenghs , these behavior may by related to the different absorption mechanism for free carriers, and the The Magnetic Permeability (μ_r) decrease by the rate of (Fe) decreases.

5.5 Discussion

The compound ($Ba_xFe_{1-x}TiO_4$) (1, 0.1, 0.2, 0.3, 0.5, 0.6, 0.7,08, 0.9 and 0) shows some interesting physical properties. Decreasing Fe concentration decrease crystal sizes x and crystal spacing d between adjacent atoms. This may be explained by assuming that decreasing Fe concentration which has atoms acts as magnetic dipoles decreases repulsive magnetic force, which crystal spacing and crystal size as shown in table (4-11). Figure (4-15) and (4-17) indicates that upon decreasing Fe concentration increasing absorption coefficient and decrease the energy gap. Thus may be related to the effect of Fe on splitting of energy level, then the energy given by

$$E_g = E_c - E_v = (E_{C0} - E_{VO}) - 2\Delta E$$

$$= (E_{C0} - E_{V0}) + 2BH$$

$$\Delta E = E_0 - BH$$

This means that decreases the strength of local magnetic field, thus decreases the energy gap. This may be also explained by assuming that the magnetic field generated by Fe acts against the nano crystal forces that increase and broaden energy bands, thus decreases the energy gap. The decreases of energy gap

increases absorption and absorption coefficient as shown in figure (4-15) this may be attributed to the fact that decreasing the energy gap allows longer wave length beside the shorter wave lengths to be absorbed by electron to move from the valence to the conduction band.

The optical and electrical conductivities in figures (4-21) and (4-22) shows increase of conductivity upon Fe concentration for shorter wave lengths and the conductivity decreases upon increasing Fe concentration. The former compound are may be attributed to the fact Fe is a good conductor, increasing Fe concentration increase free electrons, thus increases conductivity although the energy gap increases. The latter case may be result from the fact that increasing Fe concentration decreases the energy gap, thus allows more electrons to bridge the energy gap.

5.6 Outlook and Future Work

1. The applications of results obtained for solar cells and light sensors should be done.
2. The range of concentrations used in the study need to be changed to see whether the relations obtained by this study or not.
3. The substrate and host matrix used to be doped with iron should be also changed by cheaper available ones.
4. The material used for doping can be replaced by other mineral like silver and copper.

References

[1] Arico AS, Bruce P, Scrosati B, Tarascon J-M, Schalkwijk WV Nanostructured materials for advanced energy conversion and storage devices. Nat Mater, 2005.

[2] Jeevanandam, J., Barhoum, A., Chan, Y.S. et al. Review on nanoparticles and nanostructured materials: history, sources, toxicity and regulations. Beilstein J. Nanotechnology 2018.

[3] Ratna Tantra, Nanomaterial characterization, Wiley & sons, Inc. first published April 2016 ISBN 97811187535460.

[4] S. Ben, "Solid State Electronic Devices'', Hall International, Inc., U.S.A, (1990).

[5] Francesco Trotta and Andrea Mele. Nanomaterials: Classification and Properties Nanosponges: Synthesis and Applications, Wiley-VCH Verlag GmbH & Co. KGaA, First Edition. 2019.

[6] Bhushan, B, Luo, D, Schricker, S.R.,Sigmung, W., Zauscher, S., Hand book of Nanomaterials properties, Heidelberg; London, Springer; 2014.

[7] J. Lu and C. P.Wong, "Recent advances in high-k nanocomposite materials for embedded capacitor application, 2008.

[8] Ealias, A.M. and Saravanakumar, M.P. A review on the classification, characterisation, synthesis of nanoparticles and their application. IOP Conf. Ser. Mater. Sci. Eng., 2017.

[9] Abdel Salam Hamdy Makhlof, Ahmed Barhoum, Fundamental of nano particles, Elsevier, 1st edition 2018.

[10] Kaviyarasu, K, Premanand D, Kennedy J, Manikandan E. Synthesis of mg doped TiO2 nanocrystals prepared by wet-chemical method: optical and microscopic studies. International Journal of Nanoscience.2013.

[11] Luisa Filipponi and Duncan Sutherland, Nano Technologies: Principles, Applications, Implications and Hands-on Activities, European Union, 2012, ISBN 978-92-79-21437-0.

[12] Neha Srivastava, Manish Srivastava, P. K. Mishra and Vijai Kumar Gupta. Green Synthesis of Nanomaterials for Bioenergy Applications, First Edition. John Wiley & Sons Ltd, 2021.

[13] Alagarasi, An introduction to Nanomaterials, Narosa publishing house, 21 November 2016.

[14] Konstantin Sobolev, Ismael Flores, Roman Hermosillo, Leticia M. Torres-Martínez, Nanomaterials and Nanotechnology for High-Performance Cement Composites, Proceedings of ACI Session on "Nanotechnology of Concrete: Recent Developments and Future Perspectives", Denver, USA, November 7, 2006.

[15] Kumar, N. and Kumbhat, S. Carbon-based nanomaterials. Essentials in Nanoscience and Nanotechnology, 189–236. Hoboken, NJ, U.S.A.: Wiley(2016).

[16] Gokarna, A., Parize, R., Kadiri, H. et al. Highly crystalline urchin-like structures made of ultra-thin zinc oxide nanowires. RSC Adv. (2014).

[17] Badrossamay, M.R., McIlwee, H.A., Goss, J.A., and Parker, K.K. Nanofiber assembly by rotary jet-spinning. Nano Lett. (2010).

[18] Zhang, J., Langille, M.R., and Mirkin, C.A. Synthesis of silver nanorods by low energy excitation of spherical plasmonic seeds. Nano Lett. (2011).

[19] Vollath D. Nanomaterials: An Introduction to Synthesis, Properties and Application. November 2008, Vol. 7, No.6, 865-870.

[20] Gleiter, H. Nanostructured materials: basic concepts and microstructure. Acta Materialia. (2000).

[21] brinker, c. Jeffrey, sol –gel science :the physics and chemistry of sol-gel processing “ , boston , academic press ,1990.

[22] Adachi, M., Kusumi, M., and Tsukui, S. Ion-induced nucleation in nanoparticle synthesis by ionization chemical vapor deposition. Aerosol Sci. Technol. 2004.

[23] Bhaviripudi, S., Mile, E., Iii, S.A.S. et al. CVD synthesis of single-walled carbon nanotubes from gold nanoparticle catalysts. J. Am. Chem. Soc. 2007.

[24] P.Prashanth ," Presentation of Thermal Evaporator " , Indian Institute of Science Publication, 2010.

[25] Lugscheider, E., Barwulf, S., Barimani, C. et al. Magnetron-sputtered hard material coatings on thermoplastic polymers for clean room applications. Surf. Coat. Technol. 1998.

[26] Amendola, V. and Meneghetti, M. Laser ablation synthesis in solution and size manipulation of noble metal nanoparticles. Phys. Chem. 2009.

[27] Yadav, T.P., Yadav, R.M., and Singh, D.P. Mechanical milling: a top down approach for the synthesis of nanomaterials and nanocomposites. Nanosci. Nanotechnol., 2012.

[28] Charles Ktile introduction to Solid State Physics 8th addition John Wiley & Sons, Inc(2005)ISBN 0-471-41526-x.

[29] Tropf, William J., Michael E. Thomas, and Terry J. Harris. "Properties of crystals and glasses." Handbook of optics 1995.

[30] N.W. Ashcroft and N.D. Mermin: Solid State Physics, HRW International Editions, 1976.

[31] Chetan. Nayak, Solid State Physics, Physics140a, University of California, September 2000.

[32] J. Pearson Solid State Physics, University of Manchester 13 may 2008.

[33] William D. Callister, Jr., Inc. Materials science and engineering: an introduction 8th addition John Wiley & Sons (2010) ISBN 978-0-470-41997-7.

[34] Jenkins RH, Snyder RL, Introduction to X-ray powder diffractometry. Wiley-Interscience, New York (1996).

[35] Vincent, A., Molecular Symmetry and Group Theory, 2nd Edn, Wiley, Chichester, UK, 2001.

[36] Teaching Space Group Symmetry through Problems" J. Chem.Edu.1997.

[37] W. Kleber, H. J. Bautsch, J. Bohm, crystallography 8^{th} ed., Oldenburg Berlin, 1998.

[38] W. Borchardt-Ott, crystallography 7^{th} ed. Springer, Berlin, Heidelberg, 2009.

[39] Mary Anne, physical properties of materials, CRC Press. 2018. ISBN 9781138605107.

[40] Dreysse, Hugues, Electric Structure and Physical Properties of Solids, Springer 2020.

[41] Lubick N, Betts K. Silver socks have cloudy lining". Environ Sci. Technol. Bibcode. (2008).

[42] Zou B., Huang C.Z., Wang J., Liu B.Q., Effect of Nano-Scale Ti Non the Mechanical Properties and Microstructure of Si_3 N_4 Based Ceramic Tool Materials, Key Eng. Mater., 2006,

[43] Wooten, F. Optical Properties of Solids. New York: Academic.1972.

[44] Woggon, U. Optical Properties of Semiconductor Quantum Dots. Berlin: Springer. 1996.

[45] M. Born and E. Wolf, “Principles of Optics,” Pergamon Press, United Kingdom, 6th ed. 1993

[46] Linda J. Vandergriff Director of Photonics System Engineering Science Applications International Corporation McLean, Virginia, 2008.

[47] A.Lipson, S.G.Lipson, H.Lipson, "Optical Physics ", Cambridge University Press, fourth edition (2011).

[48] O. Stenzel," The Physics of Thin Film Optical Spectra–an introduction ", Springer, Germany, (2005).

[49] Lange’s Handbook of Chemistry, Dean, J.A., Ed. McGraw-Hill, Inc., New York. (1992).

[50] Weast, R.C., Ed.. Handbook of Chemistry and Physics, 56th Edition, CRC Press, Cleveland. 14th Edition, (1975).

[51] D. A. Neamen," Semiconductor Physics and Devices ", University of New Mexico ,(1992)

[52] R. Ellingson and M. Heben, Absorption coefficients of semiconductor thin films, University of Toledo, October 2013.

[53] Harland G. Tompkins and James N. Hilfiker, Spectroscopic Ellipsometry, Momentum press (2015).

[54] Sirotin and M.Shaskolskays, “Fundamental of Crystal Physics” ,Mir Publishers, Moscow, (1982).

[55] Baumeister PW, Optical absorption of cuprous oxide, Physical Review, 1961.

[56] K. L. Chopra, "Thin Film Devices Application", Plenum Press,New York, (1983).

[57] N.A. Subrahamanyam, "Textbook of Optics", 9edition, 1TDelhi1TIndia, (1977).

[58] H.S. Nalwa, Handbook of Thin Films Materials, Academic Press All rights of reproduction in any form reserved, 2001.

[59] Dikshitulu K. Kalluri, principle of electromagnetic waves and materials, 2nd edition,CRC Press, Taylor and Francis group,2018, ISBN 13: 4978-1-3329-8.

[60] E.Y.Tsymbal, Optical properties of solids, academic press New York and London, 1972.

[61] L. Solymar, D. Walshr R. R. A. Syms, electrical properties of materials, Ninth edition Oxford University Press, 2014, ISBN 978–0–19–870278–8.

[62] M. K. Jayaraj, optical and electrical properties, material Horizons; from nature to nanomaterial, 1st edition 2020, ISBN. 10-98115333x.

[63] Michael B. Heaney. "Electrical Conductivity and Resistivity. "Copyright CRC Press LLC. 2000.

[64] Gonzale, W and Mancini, H.L, an introduction to materials science. Princeton University press (2004). ISBN 9780-691-07097-1

[65] Uichiro Mizutani, introduction to electron theory, Cambridge university press, 1st edition 2001 ISBN-10 0521587099.

[66] Smith AM, Nies. Semiconductor nanocrystals, structure, properties, band gap engineering. Accchem Ress 2010.

[67] Eisberg & Resnick, Quantum Physics of Atoms, Molecules, Solids, Nuclei and Particles, Wiley, Sons, Chicago style, 2nd edition, (1984).

[68] Vasyl Morozhenko, infrared Radiation, In Tech Janeza Trdine, Croatia. 1st February, 2012 ISBN 978-953-51-0060-7.

[69] Gunzler, H. and Gremlich, H.-U., IR Spectroscopy: An Introduction, Wiley-VCH, Weinheim, Ger-many, 2002.

[70] Hollas, J. M.,Modern Spectroscopy, , Wiley, Chichester, UK, 3rd Edition, 1996.

[71] N.B. Colthrup, L.H. Daly, S.E. Wiberley, Introduction to Infrared and Raman Spectroscopy, Academic Press, San Diego, 1990.

[72] Atkins, P. and de Paula, J.,Physical Chemistry, , Oxford University Press, Oxford, UK, 7th Edition 2002.

[73] Sabu Thomas, Aparna Thankppan, perovskite photovoltaics, Elsevier Inc2018.

[74] Richard J. D. Tiley, perovskite: structure – property relationships, Wiley & sons, Inc. first published 2016 ISBN 97811189535651

[75] Guang Zhu , Likun Pan, perovskite materials: synthesis, characterization, properties and application Bo D- books on Demand , 2016

[76] Shisode, M.V., et al., Investigations of magnetic and ferroelectric properties of multiferroic Sr-doped bismuth ferrite. Applied Physics A, 2018.

[77] D. Wood, "Optoelectronic Semiconductor Devices", Prentice Hall, New York, (1994).

[78] Duangdao Channei1, Auppatham Nakaruk, Sukon Phanichphant, Pramod Koshy and Charles Christopher Sorrell. Effect of iron doping on the structural and optical properties of CeO2films, Springer Science and Business Media New York 2016.

[79] J. O. Carneiro. S. Azevedo, F. Fernandes, E. Freitas, M. Pereira, C. J. Tavares, and S. Lanceros-Mendez and V. Synthesis of iron-doped TiO2nanoparticles by ball-milling process: the influence of process parameters on the structural, optical, magnetic, and photocatalytic properties, Springer Science+ Business Media New York 2014.

[80] Stephen Lourduraj and Rayar Victor Williams Effect of iron doping on structural and optical properties of TiO_2 thin film by sol–gel routed spin coating technique J. Adv. Dielect. 7, 1750024 (2017).

[81] BS Avinash, VS Chaturmukh, HS Jayanna, and CS Naveen, effect of particle size on band gap and DC electrical conductivity of TiO_2 nanomaterial, 2016.

[82] L.H Omari and H. Lassri, Structural and optical properties of Fe-doped ruddlesden – popper Ca_3 $Ti_{2-x}Fe_x$ $O7_{-\delta}$ nanoparticles Elsevier B. V. 2020.

[83] Nicholas O. Ongwen, Andrew O.Oduor1, and Elijah O. Ayieta, Effect of Concentration of Reactants on the Optical Properties of Iron Doped Cadmium Stannate Thin Films Deposited by Spray Pyrolysis; Published by Scientific & Academic Publishing 2019.

[84] Faycal Bourguibal, Ahmed Dhahri, TarekTahri, Kamel Taibi, Jemai Dhahrii, and Ekhlil, Structural, optical spectroscopy, optical conductivity and dielectric properties of $BaTi_{0.5}$ $Fe_{0.33}$ $W_{0.17}$ O_3perovskite ceramic, Bull. Mater. Sci., Vol. 39, No. 7, Indian Academy of Sciences December 2016.

[85] Abbas Hiader Hussein, Study Structural and Optical Properties of Cd Se: Al Thin Films as a Function of Doping Ratio and Annealing Temperature, University of Anbar, Iraq 1998.

[86] Fatima Zahra Chafi, Lahoucine Bahmad, Najem Hassanaini, Boubker Faresi, and Larbi Laanab Characterization techniques of Fe-doped CuO thin films deposited by the Spray Pyrolysis method, Mohammed V University, Morocco,

[87] Dhananjay N. Bhoyar, Sandeep B. Somvanshi, P. B. Nalle1, V. K. Mande, A.A. Pandit, and K. M. Jadhav. Multiferroic Fe^{3+} ion doped

$BaTiO_3$ Perovskite Nano ceramics: Structural, Optical, Electrical and Dielectric Investigations, IOP Publishing Ltd, 2020.

[88] Linhua Xua and Xiangyin Li, Influence of Fe-doping on the structural and optical properties of ZnO thin films prepared by sol–gel, ournal homepage, Elsevier B.V. All rights reserved 2010.

[89] Infrared Spectroscopy: Fundamentals and Applications B. Stuart,John Wiley & Sons, Ltd 2004, ISBNs: 0-470-85427-8.

[90] Griffiths, P. R. and de Haseth, J. A., Fourier Transform Infrared Spectrometry, Wiley, New York, 1986.

[91] Perkampus, Heinz-Helmut, UV-VIS Spectroscopy and Applications, Springer Lab Manuals, 1992.

[92] Ujjwal, A K Sen, UV-VIS Spectroscopy: absorption Spectroscopy, Lab Lambert Academic